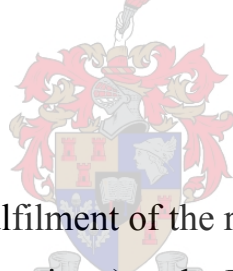


SUPPLY-DEMAND ANALYSIS OF ENERGY  
METABOLISM IN *LACTOCOCCUS LACTIS*  
UNDER ANAEROBIC CONDITIONS

Sandra Jordaan



Thesis presented in partial fulfilment of the requirements for the degree of  
Master of Science (Biochemistry) at the University of Stellenbosch

Supervisor: Prof. J.M. Rohwer

Co-supervisor: Prof. J.L. Snoep

December 2011

## DECLARATION

By submitting this thesis/dissertation electronically, I declare that the entirety of the work contained therein is my own, original work, and that I have not previously in its entirety or in part submitted it for obtaining any qualification.



---

Signature

27/09/2011

---

Date

## SUMMARY

The interests in understanding the metabolic processes of microbial systems are numerous. The interest in the species *Lactococcus lactis* (*L. lactis*) lies in applications to the food industry and in studies comparing the metabolism of related organisms.

The aim of this study was to perform *in vivo* supply-demand analysis on anaerobically fermenting *L. lactis*. This was done by perturbing both the supply and demand pathways, then measuring glycolytic flux (by means of  $^{13}\text{C}$  NMR spectroscopy) and intracellular ATP/ADP (by means of  $^{31}\text{P}$  NMR spectroscopy) at *steady state* – where the central metabolite, ATP, is produced at the same rate as it is consumed and its concentration thereby remains constant. The *L. lactis* reference strain MG1363 was supplemented with glucose and analysed “online” by  $^{13}\text{C}$ -NMR under anaerobically-fermentative conditions. The rates of glucose consumption and lactate production were determined from this  $^{13}\text{C}$  flux. Due to experimental difficulties with the online detection of  $^{31}\text{P}$  (possibly due to the low biomass yield and the choice of growth medium), ATP/ADP levels had to be determined offline: from the same batch cultures as the  $^{13}\text{C}$  samples, fermentations were performed and halted at time points when the cells had attained a steady state. These fermentation cultures were then subjected to cell lysis and centrifugation in order to extract intracellular metabolites. These cell extracts were analysed offline by  $^{31}\text{P}$  NMR in order to determine levels of phosphate metabolites, specifically ATP and ADP.

Perturbation of the supply pathway was achieved by utilising a genetically modified strain (the CS8 strain with over-expressed *las* operon) and comparing it to the reference strain MG1363. This resulted in a slight increase in ATP/ADP, but also yielded a slightly reduced flux, which is contrary to expectations from a mutant with over expressed glycolytic enzymes.

The demand pathway was perturbed by two methods: 1) utilising a genetically modified strain (the BK1506 strain with over-expressed  $F_1$ -ATPase) and comparing it to the reference strain MG1363, and 2) by treating wild-type MG1363 with sodium acetate and

comparing flux and ATP/ADP values to the untreated wild-type. Sodium acetate dissociates in the cytoplasm and causes dissipation of the transmembrane proton motive force, which is re-established by upregulation of membrane-bound H<sup>+</sup>-translocating ATPases. While the use of genetically modified strains provided only one flux-vs-ATP/ADP data point to compare to the wild-type (not sufficient for complete supply-demand analysis), the treatment of the wild type with uncoupler yielded several data points where flux and ATP/ADP values differed according to the concentration of uncoupler added.

The CS8 strain demonstrated a 19 % reduced glucose flux (24 % reduced lactate flux) with respect to the wild type MG1363. The BK1506 strain demonstrated a 72 % increase in glucose flux (33 % increase in lactate flux) with respect to the wild type. The treatment with 2 mM acetate resulted in a 72 % increase in glucose flux (123 % increase in lactate flux), whereas treatment with 4 mM acetate resulted in a 107 % and a 126 % increase in glucose and lactate fluxes, respectively. The treatment with different concentrations of acetate provided several data points with corresponding flux and ATP/ADP, enabling the calculation of the elasticity coefficient of the supply pathway to changes in ATP/ADP ( $\epsilon_{\text{ATP/ADP}}^{\text{supply}}$ ) which was found to be -5.6 and -6.3 for glucose and lactate, respectively.

The elasticity coefficient was high compared with values obtained in similar studies on other organisms. Considering that at steady state the supply and demand fluxes are equal, the high supply elasticity (which is easier to measure), when incorporated into control coefficient summation theorems, gives the indication that: 1) a greater amount of control may reside in the ATP demand pathway (the elasticity of which is more difficult to determine experimentally, but which may well be lower than the supply elasticity), and 2) ATP/ADP homeostasis is good, as indicated by a high elasticity of the supply pathway to ATP/ADP. This study represents a basis for further supply-demand analysis with non-growing batch cultures of *L. lactis*.

## OPSOMMING

Daar is groot belangstelling daarin om die metaboliese prosesse van mikrobiële sisteme beter te verstaan. Die belang van die spesie *Lactococcus lactis* (*L. lactis*) lê beide in die toepassing in die voedselbedryf en in studies wat die metabolisme van verskeie organismes vergelyk.

Die doel van hierdie studie was om *in vivo* vraag-aanbod analise uit te voer op anaerobies-fermenterende *L. lactis*. Dit was gedoen deur beide die aanbod en vraag reaksie-blokke te moduleer en dan die glikolitiese fluksie (d.m.v.  $^{13}\text{C}$  KMR spektroskopie) en die intrasellulêre ATP/ADP (d.m.v.  $^{31}\text{P}$  KMR spektroskopie) in 'n bestendige toestand te meet (wanneer die sentrale metaboliet, ATP, teen dieselfde tempo geproduseer en verbruik word en sy konsentrasie daardeur konstant bly). Die *L. lactis* verwysing-stam MG1363 is met glukose aangevul en  $^{13}\text{C}$  fluksie is aanlyn onder anaerobies-fermenterende kondisies gemeet. Die tempo van glukose verbruik en laktaat produksie is vanaf die  $^{13}\text{C}$  fluksie bereken. Eksperimentele probleme met die aanlyn bepaling van  $^{31}\text{P}$  (dalk as gevolg van lae biomassa en/of die keuse van groeimedium) moes ATP/ADP vlakke af-lin indirek bepaal word: fermentasies van dieselfde lot-kulture as die  $^{13}\text{C}$  monsters is opgestel en by sekere tydpunte gestop wanneer 'n bestendige toestand bereik was (waar ATP/ADP konstant bly). Hierdie fermenterende kulture is blootgestel aan sel-lise en sentrifugasie om intrasellulêre metaboliete te onttrek. Dié sel-ekstrakte is deur  $^{31}\text{P}$  KMR geanaliseer om die vlakke van fosfaat metaboliete, spesifiek ATP en ADP, te bepaal.

Die aanbod blok is gemoduleer deur gebruik te maak van 'n geneties-gemodifiseerde stam (die CS8 stam met 'n ooruitgedrukte *las* operon) en met die verwysing stam MG1363 te vergelyk. Dié gemuteerde stam het 'n effense toename in ATP/ADP getoon, maar het gelyktydig ook 'n afname in glikolitiese fluksie getoon, wat onverwags is vir 'n stam met ooruitgedrukte glikolitiese ensieme.

Die vraag blok is met twee metodes gemoduleer: 1) deur gebruik te maak van 'n geneties-gemodifiseerde stam (die BK1506 stam met 'n ooruitgedrukte  $F_1$ -ATPase), en 2) deur die wildetipe MG1363 met natrium asetaat te behandel en daardeur ATP verbruik van biomassa produksie te ontkoppel en die vraag na ATP te vermeerder. Daarna word die fluksie en ATP/ADP waardes met die onbehandelde wildetipe vergelyk. Natrium asetaat dissosieer in die sitoplasma en verswak die transmembraan elektriese potensiaal, wat dan weer versterk word deur membraan-gekoppelde  $H^+$ -ATPase ensieme wat protone uit die sitoplasma uit pomp. Terwyl die gebruik van geneties-gemodifiseerde stamme net een fluksie-tot-ATP/ADP datapunt voorsien om met die wildetipe te vergelyk (wat nie voldoende is vir totale vraag-aanbod analise nie), het die behandeling van die wildetipe met ontkoppelaar meerdere datapunte voorsien waar fluksie en ATP/ADP waardes verskil volgens die konsentrasie van ontkoppelaar wat bygevoeg is.

Die CS8 stam het 'n 19 % verminderde glukose fluksie getoon, asook 'n 23 % verminderde laktaat fluksie, in vergelyking met die wilde tipe MG1363. Die BK1506 stam het 'n 73 % toename in glukose fluksie getoon, asook 'n 34 % toename in laktaat fluksie, in vergelyking met die wilde tipe. Behandeling met 2 mM natrium asetaat het 'n 64 % toename in glukose fluksie veroorsaak, sowel as 'n 124 % toename in laktaat fluksie, en behandeling met 4 mM natrium asetaat het 108 % toename in glukose fluksie en 127 % toename in laktaat fluksie veroorsaak. Behandeling met verskillende konsentrasies natrium asetaat het genoeg data punte (fluksies met toepaslike ATP/ADP waardes) verskaf om die berekening van elastisiteits-koëffisiënt van die aanbod reaksie-blok tot veranderinge in ATP/ADP ( $\epsilon_{ATP/ADP}^{supply}$ ) te bereken. Die waardes was -5.6 vir glukose fluksie en -6.3 vir laktaat fluksie.

Die elastisiteits koëffisiënt was relatief hoog in vergelyking met waardes wat in soorteglyke studies op ander organismes bepaal is. Aangesien die fluksies van die aanbod en vraag reaksie blokke by 'n bestendige toestand dieselfde tempo het, kan die hoë waarde van die aanbod elastisiteits-koëffisiënt (wat die makliker een is om te meet) na die volgende afleidings lei: 1) meer kontrole mag in die ATP verbruikende reaksie-blok geleë wees (die elastisiteits-koëffisiënt is moeiliker om eksperimenteel te bepaal maar

mag wel laer as die aanbod-elasticiteit wees), en 2) ATP/ADP homeostase word goed gehandhaaf, soos aangetoon deur die hoë aanbod-elasticiteit. Hierdie studie dien as 'n basis vir verdere vraag-aanbod analise in nie-groeiende *L. lactis* lot-kulture.

To my Mom and Dad, for their unfailing love and support, and for leading  
by example, with dynamism and commitment.



## ACKNOWLEDGEMENTS

I would like to thank:

Prof Johann Rohwer, my supervisor: for his patient and systematic approach in guiding my maturation as a scientist and researcher, and for going out of his way to meet with me afterhours (and some quite early mornings).

Prof Jacky Snoep, my co-supervisor: for his valuable insight into particulars of my project and invaluable feedback on my work.

Mr Arrie Arends: for seamless lab management, comprehensive training, end-less patience, great moral support and superb crisis management.

Jean McKenzie, Elsa Malherbe and Dr. Jaco Brand for technical and theoretical assistance with the NMR component of my experimental work.

Colleagues and friends at the US Department of Biochemistry: for the huge amounts of moral support, useful discussions and occasional back-up when I had a lot on my plate.

Family and friends who have no professional relation to this project, but without whom this thesis would have been far more difficult to complete.

The National Research Foundation of South Africa for funding for this project.

## CONTENTS

ABBREVIATIONS .....	xiii
CHAPTER 1: .....	1
INTRODUCTION .....	1
1.1. <i>Lactococcus lactis</i> .....	1
1.1.1 Traditional applications .....	1
1.1.2 Modern applications.....	2
1.1.3 Physiology and biochemistry of <i>L. lactis</i> .....	2
1.2 Glycolysis in <i>L. lactis</i> ssp <i>cremoris</i> .....	3
1.2.1 Sugar uptake.....	3
1.2.2 Emden-Meyerhof-Parnas pathway.....	4
1.2.3 Fermentation patterns.....	7
1.3 Modelling of glycolysis in <i>L. lactis</i> .....	9
1.4. Analysing metabolism .....	10
1.4.1 Metabolic control analysis (MCA) .....	10
1.4.2 Supply-demand analysis .....	15
1.4.3 Enzymes influencing supply-demand in <i>L.lactis</i> .....	18
1.4.4 Implications for this study .....	22
1.5 Nuclear magnetic resonance spectroscopy .....	23
1.5.1 Theory of NMR.....	23
1.5.2 Practical NMR spectroscopy.....	28
1.5.3 Biological applications of NMR spectroscopy .....	32
1.6 Aims and outline of this thesis.....	34
CHAPTER 2: .....	35
STANDARDS AND CALIBRATIONS .....	35
2.1 Growth rates of <i>L.lactis</i> strains .....	35
2.2 Dry weight .....	37
2.3 NMR standards .....	38
2.3.1 <sup>13</sup> C NMR: Glucose standards.....	38

2.3.2 <sup>31</sup> P NMR: ATP and ADP standards .....	40
2.4 Relaxation-time calibrations .....	44
2.4.1 <sup>13</sup> C relaxation delay calibrations .....	44
2.4.2 <sup>31</sup> P relaxation delay calibrations .....	46
CHAPTER 3: .....	48
PERTURBING ATP SUPPLY AND DEMAND IN NON-GROWING FERMENTING <i>L. LACTIS</i> .....	48
3.1 Introduction to experimental results .....	48
3.2 <sup>13</sup> C NMR for flux determination .....	49
3.3 <sup>31</sup> P NMR for ATP/ADP determination .....	54
3.4 Supply-demand analysis .....	56
CHAPTER 4: .....	60
DISCUSSION .....	60
4.1 Synopsis .....	60
4.2 Discussion .....	60
4.2.1 NMR as analytical technique .....	60
4.2.2 Wild-type fermentation patterns .....	61
4.2.3 Lactate production .....	62
4.2.4 Demand perturbations .....	63
4.2.5 Supply perturbation .....	69
4.3 Future Work .....	70
4.4 Conclusions .....	71
CHAPTER 5: .....	72
MATERIALS AND METHODS .....	72
5.1. Culture methods ( <i>Lactococcus lactis</i> ) .....	72
5.1.1 Bacterial strains .....	72
5.1.2 Culture media .....	72
5.1.3 Stocks .....	72
5.1.4 Bacterial cell culture .....	72
5.1.5 Cell harvesting .....	73

5.1.6 Reagents.....	73
5.2 $^{13}\text{C}$ NMR spectroscopy: Carbon fluxes.....	73
5.2.1 In vivo fermentations.....	73
5.2.2 Concentrations of $^{13}\text{C}$ metabolites from NMR data.....	74
5.3 $^{31}\text{P}$ NMR spectroscopy: ATP/ADP determination.....	74
5.3.1 Fermentations and cell extracts.....	74
5.3.2 In vitro phosphate-metabolite measurements.....	75
5.3.3 ATP/ADP ratios from NMR data.....	75
5.4. Supply-demand analysis.....	75
REFERENCES.....	76

## ABBREVIATIONS

1,3-PG	1,3-Diphosphoglycerate
2-PG	2-Phosphoglycerate
3-PG	3-Phosphoglycerate
ALdec	Acetolactate decarboxylase
Ac-CoADH	Acetyl-Coenzyme A dehydrogenase
Acet	Acetoin
Acetyl-CoA	Acetyl Coenzyme A
AcK	Acetate kinase
AcLac	Acetolactate
AR	Acetoin reductase
ADP	Adenosine diphosphate
ADH	Alcohol dehydrogenase
ALD	Aldolase
AMP	Adenosine monophosphate
AS	Acetolactate synthetase
ATP	Adenosine triphosphate
But	2,3-Butanedione (Di-acetyl)
DHAP	Dihydroxyacetone-phosphate
EDTA	Ethylenediamine tetra-acetic acid
Eno	Enolase
FBP	Fructose-1,6-bisphosphate
For	Formate
Galac	Galactose
GAP	Glyceraldehyde-3-phosphate
GAPDH	Glyceraldehyde-3-phosphate dehydrogenase
Glc	Glucose
HK	Hexokinase

Lac	Lactose
LDH	Lactate dehydrogenase
MCA	Metabolic control analysis
MES	Morpholino-ethanesulphonic acid
NAD <sup>+</sup>	Nicotineamide adenine dinucleotide (oxidised)
NADH	Nicotineamide adenine dinucleotide (reduced)
NMR	Nuclear magnetic resonance
PFL	Pyruvate formate lyase
PDH	Pyruvate dehydrogenase
PEP	Phosphoenolpyruvate
Perm	Permease
PFK	Phosphofructokinase
PGI	Phosphoglucose isomerase
PGK	Phosphoglycerate kinase
PGM	Phosphoglycerate mutase
PK	Pyruvate kinase
PTA	Phosphotransacetylase
PTS	Phosphoenolpyruvate-dependent phosphotransferase systems
Pyr	Pyruvate
Tag	Tagatose
Tag-6-P	Tagatose-6-phosphate
TDP	Tagatose diphosphate
TEP	Triethyl phosphate
TIM	Triose phosphate isomerase

## CHAPTER 1: INTRODUCTION

The application of mathematical tools to describe living systems has great industrial value by enabling the prediction of biological responses to changes in internal or external parameters. While these predictions are essentially theoretical, they do reduce the need for time- and resource-consuming experiments. Furthermore, it enables the *in silico* identification of potential targets for perturbation, the experimental identification of which would be far more time-consuming. Construction of such a model relies on the selection of model organisms to generate experimental data, from which variables and parameters can be quantified.

This study involves experimental investigation of the control of free-energy supply and demand in the model organism *Lactococcus lactis* in the context of a metabolic control analysis approach. Quantification of glycolytic flux and the corresponding energy state of the cell under various conditions enabled the calculation of rate characteristics and determination of control over the steady state glycolytic flux.

### **1.1. *Lactococcus lactis***

#### *1.1.1 Traditional applications*

In many African cultures, milk has for centuries traditionally been fermented, both for the purpose of preservation and for flavour. Such fermentation practices, involving treatment of fermentation containers with a bacterial inoculum, date back through many generations [1, 2]. One of the genera of microbes most prevalent in bacterial inocula is the *Lactococcus* family. In South Africa, *Lactococcus* has been found to comprise part of the five most dominantly-featuring genera in microbial isolates from traditional milk fermentation methods [1]. In a similar study on traditional milk fermentation practices in Burkina Faso (North-Western Africa) *Lactococcus* was found to comprise 20 % of dairy inoculation mixtures [3]. *Lactococcus* can therefore be considered one of the most widely and commonly used genera in indigenous food fermentation techniques.

### 1.1.2 Modern applications

In the last decade of the 19th century, European and North American scientists noted the existence of naturally-occurring bacterial populations within the udders of cows, which are also present in the freshly-drawn milk [4]. Later studies [5, 6, 7] have established that some of the bacteria found in raw milk are pathogenic and are responsible for the spoiling of untreated milk, which provides ideal conditions for the growth of bacteria. The inoculation of milk with bacteria that do not cause spoiling can prevent growth of pathogenic bacteria and preserve milk for longer [8]. Furthermore, milk fermented extensively with the use of lactic acid bacteria forms a curd, which is used for the production of cheese.

Starter cultures of lactic acid bacteria are used extensively in the food industry – particularly in the dairy industry [8-11]. The starter cultures break down lactose to (predominantly) lactate and serve to acidify milk and reduce growth of pathogenic species [12, 13]. This has a preserving effect, reducing the need for added artificial preservatives [10]. Other end-products of lactose fermentation are commonly utilised for flavour enhancement of dairy products such as flavoured milks, yoghurts, cheeses and cream [12].

The species *Lactococcus lactis*, which is commonly used in starter cultures, is an excellent model organism for supply-demand analysis because of the simplicity of its glycolytic conversion of glucose to pyruvate – and to lactate, during homolactic fermentation (Section 1.2). The characteristics of this species are described in greater detail in Section 1.1.3.

### 1.1.3 Physiology and biochemistry of *L. lactis*

The species *Lactococcus lactis* includes the formerly-classified species *Streptococcus lactis* (and all subspecies), *S. garvieae*, *S. plantarum*, *S. raffinolactis*, *Lactobacillus xylois* and *Lactobacillus hordniae* [14]. These genera of eubacteria are believed to have evolved ~2 billion years ago during the formation of the earth's oxygen, nitrogen and carbon dioxide rich atmosphere [9]. *Lactococci* are Gram-positive, neutrophilic cocci and



are the most thoroughly characterized of all lactic acid bacteria, in terms of their genome and metabolism [15].

On a microbial level, *L. lactis* cells form only short chains, or even remain in pairs [1]. In general, *Lactococci* display a preference for mild growth conditions, with poor tolerance for high temperatures, high pH and salt. Two of the major sub-species, *L. lactis* ssp *lactis* and *L. lactis* ssp *cremoris*, differ in their adaptability to environmental changes and various substrates. *L. lactis* ssp. *lactis* has numerous plant and animal sources. However, *L. lactis* ssp. *cremoris* appears to occur naturally only in the cow's tail, the cow's body, and the first and second colostrum [11]. *L. lactis* ssp. *lactis* can survive on a variety of substrates other than lactose and glucose – including maltose, ribose and arginine [16]. Both species are able to survive at temperatures as high as 40 °C and 4 % sodium chloride, as well as conditions ranging from pH 5.5-9.5 [16, 17]. *L. lactis* ssp *cremoris*, however, requires the optimal temperature of 30 °C and pH 6.3-6.9 in order to flourish [18, 19]. Both species demonstrate a reduction in biomass production in response to medium acidification as a result of their own acid-producing metabolism [18, 20]: homolactic fermentation by *L. lactis* ssp *cremoris* has been found to result in medium acidity of around pH 4-5 in low buffer concentrations.

The substrate preference and glycolytic pathways of *L. lactis* ssp. *cremoris* is described in the next section. The *Lactococcus* strain utilised in this study was *L. lactis* ssp. *cremoris* strain MG1363 [15].

## **1.2 Glycolysis in *L. lactis* ssp *cremoris***

### *1.2.1 Sugar uptake*

While *L. lactis* ssp *lactis* is able to metabolise a large variety of sugars, *L. lactis* ssp *cremoris* strain MG1363 displays a preference for glucose, galactose or lactose (a disaccharide of glucose and galactose, linked by a  $\beta$ -1,4 glycosidic bond) as substrates. All these sugars enter the cell either by means of a permease or by means of a phosphoenolpyruvate (PEP)-dependent phosphotransferase system (PTS), during which each molecule is phosphorylated to sugar-6-phosphate. Lactose is then hydrolysed by  $\beta$ -

galactosidase to produce galactose-6-phosphate and glucose, while glucose-6-phosphate directly enters glycolysis (Figure 1.1). Galactose-6-phosphate enters the tagatose pathway, producing DHAP and GAP, which then enter glycolysis at the triose phosphate level [21]. Galactose entering the cytosol via a permease is subsequently phosphorylated and enters glycolysis via the Leloir pathway as glucose-6-phosphate.

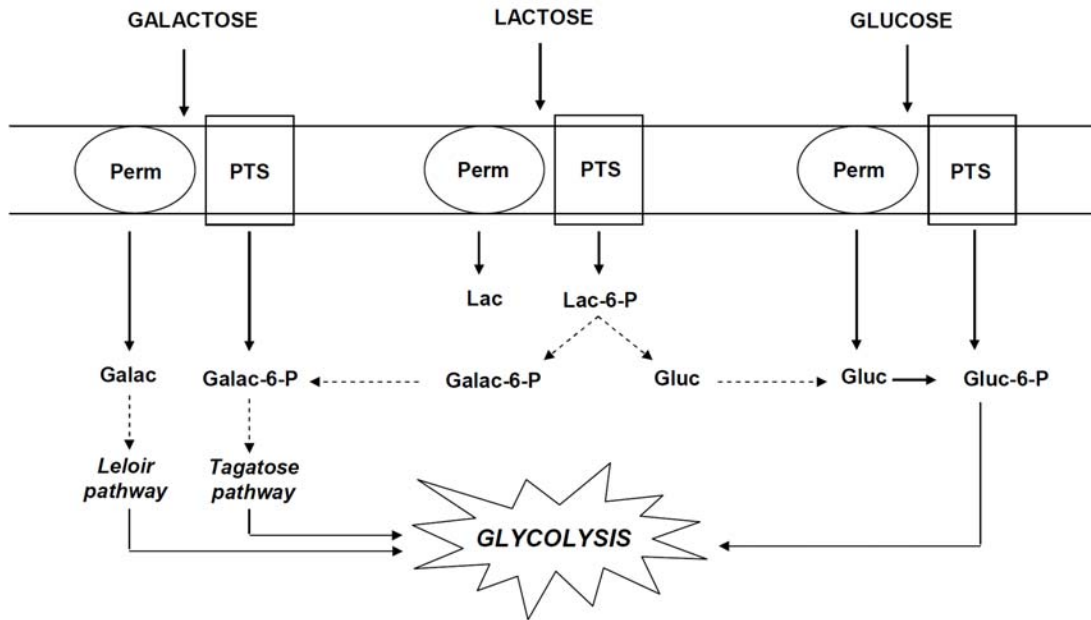


Figure 1.1. Transport of sugars into the cytoplasm in *L. lactis*.

### 1.2.2 Emden-Meyerhof-Parnas pathway

As described in a review [21], anaerobic fermentation of glucose by *L. lactis* occurs by means of the Emden-Meyerhof-Parnas pathway (Figure 1.2) [12, 22]. Glucose is phosphorylated to glucose-6-phosphate and proceeds through glycolysis to pyruvate. Two molecules of ATP are consumed in the metabolism of glucose to pyruvate: one during the phosphorylation of glucose to G-6-P by hexokinase (HK), and one at the phosphorylation of F-6-P to F-1,6-BP (FBP) by PFK. Each molecule of FBP is cleaved into two triose phosphate (GAP or DHAP) molecules and two molecules of ATP are generated per triose phosphate molecule: one at the dephosphorylation of 1,3-BPG to 3-PG by PGK and another at the dephosphorylation of PEP to pyruvate by PK. This results in the net generation of two molecules of ATP shown in the overall stoichiometric equation [Eq. 1].

Pyruvate can then enter a number of enzymatically catalysed pathways to yield a variety of products, of which the most favourable in the wild-type organism, under mild conditions with substrate abundance, is fermentation to lactate [21, 22].

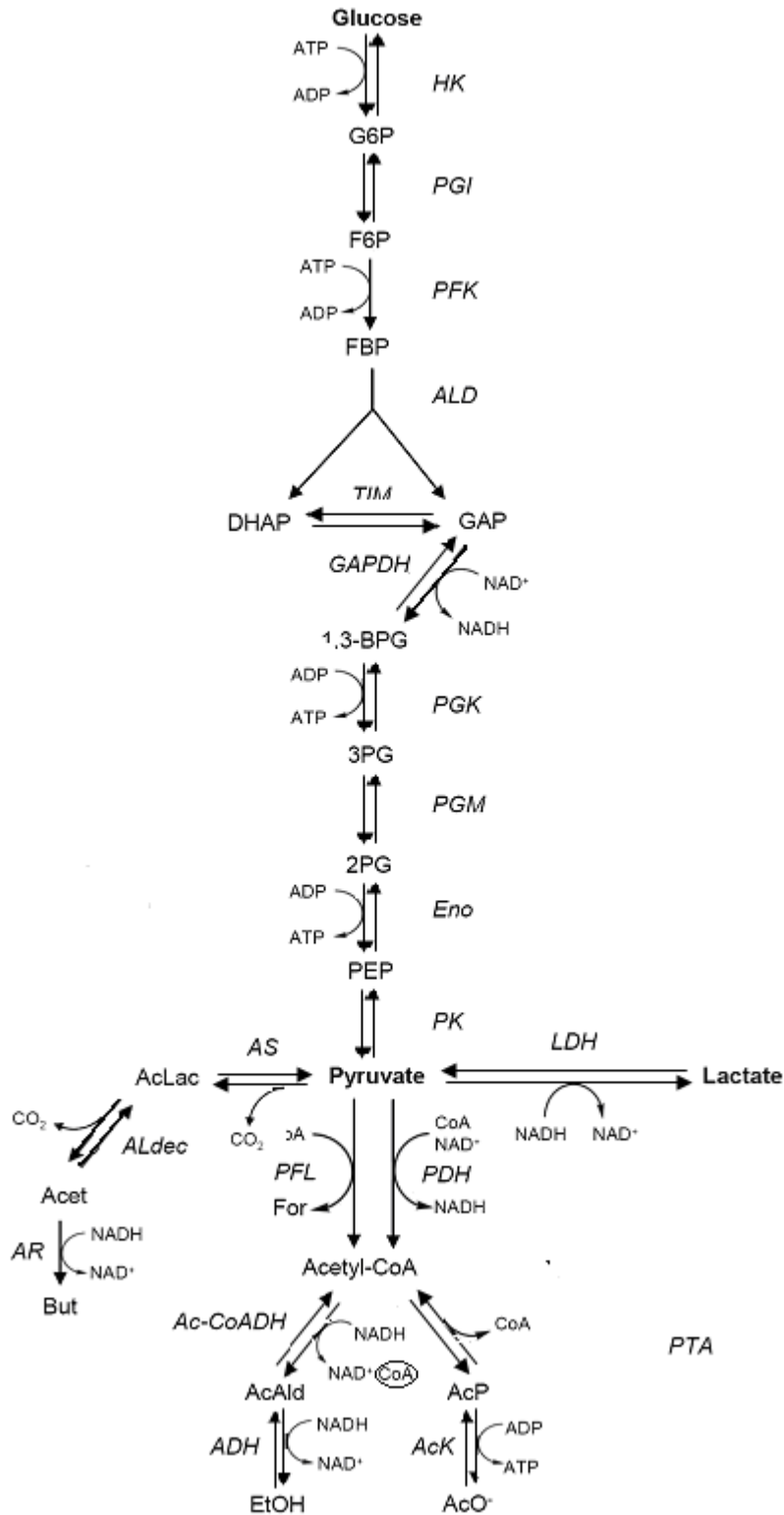
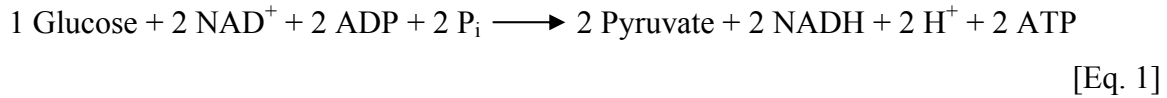
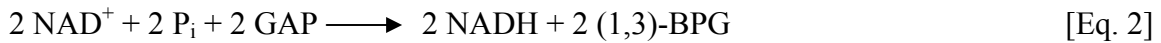


Figure 1.2. Glucose metabolism in *Lactococcus lactis* (see Abbreviations for full metabolite and enzyme nomenclature).

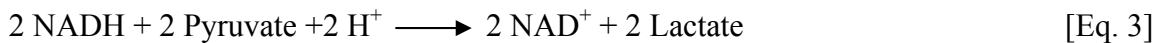
The overall stoichiometry of the catabolism of a single glucose molecule to pyruvate is as follows [23]:



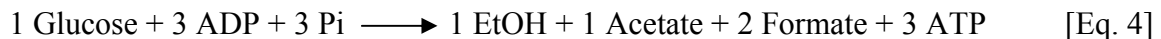
The two molecules of NADH per molecule glucose result from the oxidation (accompanied by phosphorylation) of glyceraldehyde-3-phosphate (GAP) to 1,3-bisphosphoglycerate (1,3-BPG):



Pyruvate is reduced to lactate via lactate dehydrogenase, oxidising NADH to NAD<sup>+</sup> and closing the redox cycle [10, 24].



Grown on glucose or lactose, *L. lactis* produces predominantly lactate by anaerobic fermentation [24-26]. Growth on slower-fermenting sugars results in a shift to a more mixed-acid fermentation profile [24, 26]:



Major factors influencing the fermentation profile (such as availability of substrate, pH and the ratio of redox metabolites) will be discussed in more detail in the following section.

### 1.2.3 Fermentation patterns

The ratio of the redox partners NADH and NAD<sup>+</sup> is suspected to play an important role in controlling the changes in fermentation profile between homolactic and mixed-acid fermentation in *L. lactis*. A low NADH/NAD<sup>+</sup> ratio has been found to inhibit lactate

dehydrogenase, favouring mixed-acid forming reactions, such as those catalysed by pyruvate-formate lyase and pyruvate dehydrogenase. Several theories have been raised as to the conditions under which a low NADH/NAD<sup>+</sup> ratio – and concomitant mixed-acid fermentation – normally occurs:

The ratio of products formed appears to depend on the type and accessibility of substrate, growth conditions (e.g. pH), metabolite ratios and the specific *L. lactis* strain [24, 25]. In continuous culture studies on *L. lactis* ssp. *lactis*, Starrenberg & Hugenholtz [27] observed homolactic fermentation of pyruvate to lactate under conditions of lactose abundance (over 90% when pH was below neutral), while mixed-acid fermentation was observed under starvation (substrate limitation) conditions. Products of this non-homolactic fermentation included ethanol, formate and acetate.

The results echoed the findings of a study involving *Streptococcus lactis* (re-classified as *L. lactis* ssp. *lactis* [14]), using glucose as substrate. Homolactic fermentation appears to predominate during growth on glucose, whereas growth on maltose and galactose (slowly fermenting sugars) seem to result in mixed-acid fermentation (see [Eq. 4]) [25-26, 28-29]. In the presence of excess glucose, over 80 % of glucose was converted to lactate. Glucose limitation resulted in a transition from homolactic to mixed-acid fermentation, resulting in the production of ethanol, formate and acetate [27]. However, cells that had been transferred to glucose-limited medium for some time and were then transferred to glucose-containing buffer quickly recovered their homolactic fermentation pattern.

These findings suggest that substrate type, availability and uptake into the cytoplasm affect the levels of metabolites and thereby the flux of these metabolites through glycolysis. A reduced flux, accompanied by a lowered NADH/NAD<sup>+</sup> ratio [24], may inhibit reduction of pyruvate to lactate and rather channel pyruvate toward oxidising reactions.

### 1.3 Modelling of glycolysis in *L. lactis*

Perturbing one or more steps of glycolysis to increase production of desirable products is of great value to the food industry. However, doing this experimentally can be time-consuming and complex. Not all enzymes in the glycolytic pathway have the same amount of control over the flux through the pathway. Some enzymes have greater control, meaning increases or decreases in their activity would greatly affect the direction and/or magnitude of the flux, while others have a lesser effect on the pathway flux. The influence an enzyme has on the pathway can be quantified by means of metabolic control analysis (MCA). MCA is discussed in more detail in Section 1.4 of this work, as it is the tool on which the construction of a theoretical kinetic model is based.

A kinetic model of the *L. lactis* glycolytic pathway and the associated pyruvate branches was constructed in 2002 with the aim of theoretically predicting the effect of perturbations of glycolytic parameters on the glycolytic flux [30]. The model [31] consists of the 28 reactions making up glycolysis and polysaccharide synthesis [22]. The authors used the Gepasi software [32] to simulate the model, but its availability in SBML format [33, 34] allows it to be simulated on various modeling platforms. A combined approach was used, involving kinetic modeling, metabolic control analysis (MCA) and experimental analysis, using integrated data acquired with *L. lactis* under different conditions as well as kinetic data from other organisms. The model incorporates allosteric inhibitors and activators, such as FBP, as well as feedback metabolites.

The application of MCA has enabled the identification of enzymes which have the largest effect on the magnitude and direction of the overall flux, hence indicating possible targets for experimental perturbation. The theory behind MCA is described briefly in the next section, as well as its adaptation to supply-demand analysis (Section 1.4.2). This is followed by a summary of the enzymatic components comprising ATP supply and demand and some background and theory on the analytical technique used to monitor metabolite levels.

## 1.4. Analysing metabolism

### 1.4.1 Metabolic control analysis (MCA)

Not only do various reactions in a pathway interact and influence one another, but reactions from different pathways have substrates or products that influence the rates of other reactions. Each enzyme in a pathway, or in a branch of a pathway, is like a tributary to a river – a change in the flux through that particular enzyme will to some extent affect the overall flux through the pathway. The extent to which each enzyme's local rate affects the overall flux can be experimentally determined and quantified by means of a component of applied mathematical theory known as *sensitivity analysis*. Sensitivity analysis is applied in a variety of fields to estimate the sensitivity of a system to changes in any of its parameters, and the effect such changes have on the state of the system [49].

A type of sensitivity analysis and a valuable tool for analysing and describing metabolic systems was developed from the research of Kacser and Burns [35-37], as well as Heinrich and Rapoport [38], known as **metabolic control analysis (MCA)**. MCA refers to the quantitative description of the influence of individual enzymes in a metabolic pathway on the overall flux of the pathway, as well as their influence on metabolite concentrations.

MCA requires that certain assumptions be made regarding the system being studied [37]. The most important assumptions (as summarised in [37]) include: 1) The metabolic system is treated as one unit of numerous interconnected reactions; 2) The source of initial substrate and destination of final product are referred to as “pools” and represent the “boundaries” of the metabolic system. The model system is capable of attaining a steady state, where concentrations of intermediates remain constant as the rate of production of metabolites equals the rate of their consumption or degradation. A true steady state requires the system to tend towards re-establishing these metabolite concentrations even under perturbation; 3) All enzymes utilising a specific metabolite as substrate display equal affinity for the substrate; 4) Enzymes, as catalysts, are considered parameters of the system, not variables; 5) The steady state is considered unaffected by



bound metabolites – only free metabolite concentrations are taken into consideration, not total metabolite concentrations.

MCA has been extended to include hierarchical regulatory components (known as hierarchical control analysis, HCA) [39], but this will not be covered in this review. It is nevertheless important to keep in mind that components of metabolic systems are modified and regulated by several protein cascades, including signaling and transcriptional/translational processes.

Assuming that these conditions are met, it is possible to determine the magnitude of control of each enzyme over the pathway flux or metabolite concentration. This control is defined as the extent to which the overall steady-state flux of a pathway, or the concentration of a metabolite, would change if the particular enzyme's concentration or activity was increased or decreased by a certain amount. The relative change can be expressed as the fraction or percentage of change in flux or metabolite concentration resulting from a certain fractional perturbation in enzyme concentration or activity [37]. This is determined experimentally by selectively modifying the concentration/activity of a certain enzyme, either by up-regulation or by down-regulation, and measuring the new steady state variables (flux or metabolite concentrations). The variables observed are then compared to a reference (unmodified wild-type) strain of the same organism and it is deduced to what extent an amount of change in the modified enzyme's activity results in changes in steady state flux in the modified strain with respect to the wild-type organism.

The mathematical term representing this quantification of change in a property – steady state flux ( $J$ ) or metabolite concentration ( $S$ ) – resulting from the perturbation of a system parameter (e.g. external metabolite concentration) is simplified into a single symbol, the response coefficient ( $R$ ). If the parameter being modified is represented by  $x$ , the response of the system to changes in  $x$  is expressed as  $R_x$ . Since this study is limited to the measurement of glycolytic flux ( $J$ ) and the concentration of a common metabolite ( $S$ ), we focused on the terms representing the control of  $x$  on these two properties, namely  $R_x^J$  and  $R_x^S$ , respectively.

$$R_x^J = (\delta J/J) / (\delta x/x) = \delta \ln J / \delta \ln x \quad [\text{Eq. 5}]$$

$$R_x^S = (\delta S/S) / (\delta x/x) = \delta \ln S / \delta \ln x \quad [\text{Eq. 6}]$$

If the flux (or metabolite concentration) were plotted in a double-logarithmic space against the system parameter, the slope of the resulting curve represents the response coefficient of the property (flux or concentration) to the parameter.

The effect of a change in the local rate ( $v_i$ ) of a specific enzyme on steady state flux ( $J$ ) or a metabolite concentration ( $S$ ) is referred to as the control coefficient ( $C$ ). The control coefficient is a quantification of how much the flux or metabolite concentration would change in response to a perturbation in  $v_i$ :

$$C_{v_i}^J = (\delta J/J) / (\delta v_i/v_i) = \delta \ln J / \delta \ln v_i \quad [\text{Eq. 7}]$$

$$C_{v_i}^S = (\delta S/S) / (\delta v_i/v_i) = \delta \ln S / \delta \ln v_i \quad [\text{Eq. 8}]$$

From this definition, we can deduce that the control coefficient equals the percentage change in  $J$  or metabolite concentration in response to a one percent increase or decrease in rate  $v_i$ .

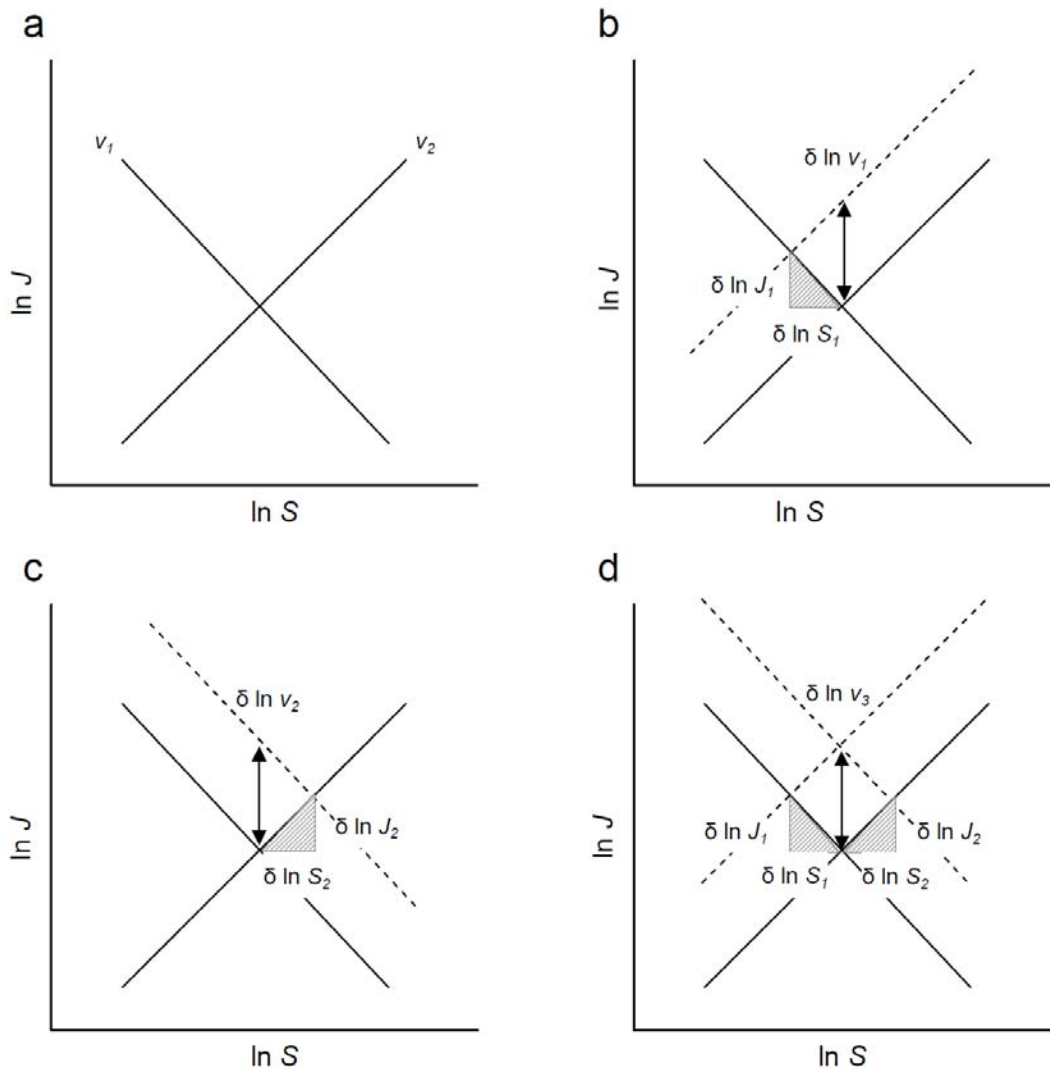


Figure 1.3. A simple system consisting of two reactions (or reaction blocks): (a) Reaction 1 producing a metabolite ( $S$ ), with a rate  $v_1$  and steady state flux  $J_1$ , and Reaction 2 consuming the metabolite ( $S$ ), with a rate  $v_2$  and steady state flux  $J_2$ . The point where the two double-logarithmic graphs intersect represents the steady state, where the fluxes of the producing and consuming pathways are equal and the concentration of  $S$  remains constant.

Should a perturbation cause an increase in the rate of reaction 1 (denoted  $\delta \ln v_1$ ), the flux would change ( $\delta \ln J_1$ ) to adopt a new steady (Figure 1.3b) with a new steady state concentration of  $S$ . A similar perturbation in the rate of reaction 2 (denoted  $\delta \ln v_2$ ),

would result in yet another steady state, with a change in flux  $J_2$  ( $\delta \ln J_2$ ) and concentration of  $S$  ( $\delta \ln S$ ) (Figure 1.3c). If both  $v_1$  and  $v_2$  were perturbed by the same magnitude (denoted  $\delta \ln v_3$ ), the change in steady state flux ( $J_3$ ) would equal the sum of the changes in flux seen for the perturbations of the individual reactions (Figure 1.3d):

$$\delta \ln J_1 + \delta \ln J_2 = \delta \ln J_3 \quad [\text{Eq. 9}]$$

In the example shown in Figure 1.3, two things hold true:

$$\delta \ln v_1 = \delta \ln v_2 = \delta \ln v_3 \quad \text{and} \quad \delta \ln J_3 = \delta \ln v_3$$

Therefore:

$$(\delta \ln J_1 / \delta \ln v_1) + (\delta \ln J_2 / \delta \ln v_2) = (\delta \ln J_3 / \delta \ln v_3) \quad [\text{Eq. 10}]$$

Using here the definition of the flux control coefficient ( $C_v^J = \delta \ln J / \delta \ln v$ ), this equation can be re-written as the **flux summation theorem**:

$$C_{v_1}^{J_1} + C_{v_2}^{J_2} = 1 \quad [\text{Eq. 11}]$$

Looking again at the example in Figure 1.3, this time at the effect of  $\delta \ln v$  on the steady state metabolite concentration ( $\delta \ln S$ ), the perturbations  $\delta \ln v_1$  and  $\delta \ln v_2$  can be seen to result in  $\delta \ln S_1$  and the  $\delta \ln S_2$ , respectively. Simultaneous (and equal) perturbations of both reaction rates lead to the following steady state equation:

$$\delta \ln S_1 = -\delta \ln S_2$$

As described above,  $\delta \ln v_1 = \delta \ln v_2 = \delta \ln v_3$ . Therefore dividing by  $\delta \ln v_3$  gives:

$$(\delta \ln S_1 / \delta \ln v_3) + (\delta \ln S_2 / \delta \ln v_3) = 0$$

This leads us to the **concentration summation theorem**:

$$C_{v1}^{S1} + C_{v2}^{S2} = 0 \quad [\text{Eq. 12}]$$

These summation theorems of MCA can be applied to a system of two reaction blocks linked by the common metabolite  $S$ . The pathway producing the metabolite is described as the “supply” reaction block, with the rate  $v_{supply}$ . Similarly, the pathway consuming the metabolite is described as the “demand” reaction block, with rate  $v_{demand}$ . For  $S$  to remain constant, such as in steady state,  $J_{supply} = J_{demand}$ . If the control coefficient summation theorem is applied to this reaction grouping, then:

$$C_{supply}^J + C_{demand}^J = 1 \quad [\text{Eq. 13}]$$

$$C_{supply}^S + C_{demand}^S = 0 \quad [\text{Eq. 14}]$$

The branch of MCA in which control analysis theory is applied to determining the distribution of flux control between the supply and demand blocks is known as **supply-demand analysis**. This approach is described in more detail in the next section.

#### *1.4.2 Supply-demand analysis*

The concept of a factory supplying a product, and the demand for this product by consumers, can be applied to supply of and demand for metabolites in living cells [40]. Metabolite concentrations are influenced by quantifiable factors, such as environmental conditions, substrate availability and enzyme activity. The realisation that a pathway (or group of pathways) producing a metabolite cannot be separated from the functional pathway (or pathways) which consumes that metabolite, led to the development of a sub-branch of MCA – namely **supply-demand analysis**.

The grouping of reactions into supply and demand pathways is only possible if the two blocks are only linked by a single common metabolite [40, 41]. In energy metabolism, the key metabolite is adenosine triphosphate (ATP), the hydrolysis of which is an exergonic reaction producing its dephosphorylated counterpart adenosine diphosphate

(ADP). The transfer of inorganic phosphate ( $P_i$ ) to ADP by kinases regenerates ATP to close the moiety-conserved cycle. Energy-requiring processes, such as ion transporters (Section 2.3.2), act as ATPases and hydrolyse ATP to  $P_i + ADP$ . Such transporters (such as membrane-bound ion translocators) “pump” excess ions out of the cytoplasm, thereby maintaining a transmembrane electrochemical gradient which is crucial in driving the cell’s anabolic processes [42].

In the supply block, glycolytic reactions result in the phosphorylation of ADP to produce ATP, which is then hydrolysed to ADP by ATPases in the demand block (Figure 1.4). ADP can be further dephosphorylated to AMP, however since AMP must first be phosphorylated to ADP before it can be converted to ATP by PGK and PK during glycolysis, it was not considered in energy-state calculations. ATP, ADP and AMP form part of a moiety-conserved cycle, where the sum of the concentrations of the partner molecules remains constant, but the ratio between the forms can vary. The normal state of a living cell is a state where the ATP/ADP ratio remains constant – i.e. ADP is phosphorylated to ATP at the same rate at which ATP is hydrolysed to ADP. This metabolic *status quo*, where the ATP/ADP ratio remains relatively constant (i.e. rate of production equals rate of demand), is known as a **steady state** (Section 1.4.1). A steady state is characterised by the rates of supply and demand pathways which constitute the maintenance of the ATP/ADP cycle.

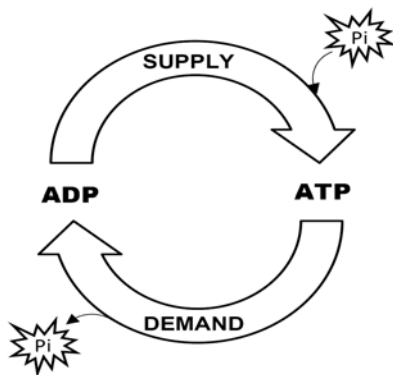


Figure 1.4. In the demand block, ATP is hydrolysed to ADP. ADP, in turn, acts as a substrate for the supply pathway to form ATP.

Each block is characterised by its own flux, with the flux of the supply block describing the rate at which substrate and ADP are converted to product and ATP, and the flux of the demand block at what rate ATP is hydrolysed to ADP and P<sub>i</sub> [40, 41].

Any changes to the rate of supply or demand (e.g. changes in enzyme activity or metabolite concentration) perturb the initial steady state and induce the cell to adapt its rates of supply and/or demand in order to compensate for this change and achieve a new steady state in which ATP/ADP ratio again remains constant.

As mentioned, the rates of the supply and demand pathways influence the concentrations of central metabolites (ATP and ADP). However, the supply and demand pathways must adapt to meet the needs of the cell. A perturbation in the supply pathway affects the ATP/ADP ratio and, depending on the sensitivity of the demand pathway to changes in ATP/ADP, would result in an increase or decrease in the demand flux in order to re-establish a steady state. Conversely, changes in the demand flux would be “felt” by the supply pathway via the ATP/ADP ratio and, depending on the sensitivity of the supply pathway to changes in ATP/ADP, the supply flux would increase or decrease in response. The quantification of the sensitivity of the supply and demand pathways to changes in the other (communicated by means of the ATP/ADP ratio) is known as the elasticity coefficient ( $\epsilon$ ) [40, 41].

The elasticity of the rate of the supply pathway ( $v_{\text{supply}}$ ) to changes in ATP/ADP is expressed as follows:

$$\epsilon_{\text{ATP/ADP}}^{v_{\text{supply}}} = \delta \ln v_{\text{supply}} / \delta \ln (\text{ATP/ADP}) \quad [\text{Eq. 15}]$$

Conversely, the elasticity of the rate of the demand pathway ( $v_{\text{demand}}$ ) to ATP/ADP is expressed as follows:

$$\epsilon_{\text{ATP/ADP}}^{v_{\text{demand}}} = \delta \ln v_{\text{demand}} / \delta \ln (\text{ATP/ADP}) \quad [\text{Eq. 16}]$$

While supply-demand analysis treats each pathway as a single reaction block, it is still important to keep in mind that each pathway is a network of reactions which share control over the pathway flux and that perturbation to a single reaction will influence other reaction rates and thereby the whole pathway. The next section describes the individual reactions, as well as interactions between the various reactions and metabolites, which make up each of the ATP supply and demand pathways.

### *1.4.3 Enzymes influencing supply-demand in *L.lactis**

#### 1.4.3.1 The ATP supply block

##### 1.4.3.1.1 Sugar uptake

Glucose is taken up by means of two distinct enzymes: 1) a phosphoenolpyruvate (PEP)-dependent phosphotransferase system (PTS), or 2) permease systems [21]. Transport of glucose by means of a PTS is accompanied by phosphorylation of glucose. Glucose entering the cytosol via a permease is phosphorylated by hexokinase as the first step of glycolysis, whereas glucose taken up by means of a PTS is phosphorylated in the process and enters glycolysis as glucose-6-phosphate. As previously mentioned, in *L. lactis* metabolism of glucose to pyruvate occurs via the Emden-Meyerhof-Parnas pathway.

In *L. lactis*, the relative importance of sugar uptake reactions in controlling the glycolytic flux has not been studied in detail, nor have allosteric activators/inhibitors involved in these processes been thoroughly identified, leaving much to be investigated with regard to sugar uptake in this organism [24].

##### 1.4.3.1.2 Glycolysis and pyruvate branches

As discussed in Section 1.2, the glycolytic flux is not only influenced by the relative concentrations of carbon intermediates, but also the ratios of reducing equivalents. The ratio of the redox co-factors NADH and NAD<sup>+</sup> plays an important role in regulating the distribution of the glycolytic flux between homolactic and mixed acid fermentation [24]. Glyceraldehyde-3-phosphate dehydrogenase (GAPDH) activity was believed to have high control on the pathway flux [43, 44], presumably via the NADH/NAD<sup>+</sup> redox cycle



[21, 24]. High GAPDH activity, such as would preside during growth on excess glucose, results in a high NADH/NAD<sup>+</sup> ratio, thereby promoting high LDH activity [24]. LDH itself showed little or no control over the glycolytic flux or conversion of pyruvate to lactate [10, 45], but high LDH activity results in predominantly homolactic fermentation [45, 46]. LDH, in turn, has been shown to be activated by high levels of FBP [25, 47], as would result from excess glucose availability [42], resulting in more homolactic fermentation in the presence of higher glucose concentrations. The saturation of GAPDH during growth on excess glucose is believed to result in some accumulation of GAP, DHAP and NAD<sup>+</sup>, which results in the inhibition of pyruvate dehydrogenase [24, 44]. However, in a study using enzyme modulation experiments, with cells growing in defined medium supplemented with glucose, small-to-moderate changes in expression of GAPDH (down to 25 % of normal activity) had no significant effect on the glycolytic flux [10].

The effect of perturbations in phosphofructokinase (PFK) activity on the pathway flux in *L. lactis* ssp *cremoris* is inconclusive [21, 47, 48]. A 62-76 % reduction in glycolytic flux was observed after a two-fold reduction in *las* operon activity (*pfk*, *ldh* and *pk*) [47]. This could be due to lowered concentrations of FBP (the product of PFK), which is an activator of LDH [23]. However, an eight-fold increase in PFK activity did not result in an increase in glycolytic flux [21]. Interestingly, despite the reduced flux observed in mutants with reduced PFK activity, fermentation remained predominantly homolactic [48]. In a further study by Koebmann *et al.* [10], PFK was found to have no control over the flux in growing cells.

An enzyme which has been attributed a high flux control role is pyruvate kinase (PK), the enzyme catalysing the conversion of phosphoenolpyruvate (PEP) to pyruvate. In *L. lactis*, PK is inhibited by P<sub>i</sub> and allosterically activated by both fructose-1,6-bisphosphate (FBP) and its substrate PEP [21, 49]. FBP has been found to increase the apparent V<sub>max</sub> of PK, as well as increase its affinity for both of its substrates, PEP and ADP. Ramos *et al.* [50] over-expressed PK and found that, although 15-fold overproduction of PK did not noticeably affect the glycolytic flux, FBP depletion appeared to continue at a high rate

beyond glucose depletion in the mutants with the over-expressed PK. It was also found that over-expression of PK resulted in the absence of the accumulation of 3-PGA and PEP that is normally found in cells under starvation conditions. Furthermore, the NADH/NAD<sup>+</sup> ratio increased markedly in the PK overproducing mutants, suggesting less efficient re-oxidation of NADH, which the authors hypothesised to result from concomitant decrease in LDH activity [49].

FBP is also a known allosteric activator of LDH and the reduction of pyruvate to lactate would presumably be favoured in high glucose conditions. Most *Lactococcus* strains display increasing tendency towards mixed-acid fermentation during growth on slowly-fermenting sugars [24]. It has been suggested that the main reason for this is that lower levels of triose phosphates results in reduced inhibition of PFL, since FBP levels were found to remain sufficiently high for full LDH activation.

In summary, the route of pyruvate metabolism is influenced by a variety of conditional factors. Abundant glucose (and efficient glucose transport) results in majority of the flux being directed towards the LDH branch. Flux limitation by low substrate availability results in re-direction of pyruvate to alternative pyruvate-consuming reactions, producing mixed-acid metabolites. Studies regarding individual enzymes have to date yielded ambiguous results, although it has been suggested that a major role in controlling the glycoytic flux is played by the sugar-transport pathways.

#### 1.4.3.2 The ATP demand block

The ability to maintain a stable cytoplasmic pH is crucial for any bacterial cell. Not only do cells require a stable intracellular environment to support biochemical functions, but a gradient must be maintained between the intracellular cytoplasm and external environment in terms of ion concentration (and therefore electrochemical charge). One very important electrochemical gradient is the proton motive force (PMF), which is dependent on an ion gradient as well as a pH gradient. The PMF drives many cellular processes, such as ion pumps and ATP synthesis [51].

One of the ways in which bacteria (including *L. lactis*) maintain their cytoplasmic pH, even in acidic conditions, is by means of a membrane-bound proton-translocation ATPase complex. This complex consists of two units [52, 53]:

- The F<sub>1</sub> unit is hydrophilic and is the catalytic site for ATP hydrolysis. It consists of five subunits, designated  $\alpha$ ,  $\beta$ ,  $\gamma$ ,  $\delta$  and  $\epsilon$ .
- The F<sub>0</sub> unit is hydrophobic in nature and spans the cell membrane, enabling passage of protons through the membrane. It, too, consists of subunits, designated a, b and c.

The precise interaction between the subunits, and their role in the proton pumping process, has not yet been fully elucidated – however, the mechanism appears to be highly conserved between species [53].

The (F<sub>1</sub>F<sub>0</sub>) proton translocating ATPase (H<sup>+</sup>-ATPase) complex functions reversibly to either synthesize ATP or to hydrolyse ATP. As mentioned before, an ion gradient exists across the cell membrane, establishing a proton motive force (PMF), which drives many energy-requiring processes in the cell. In cells lacking a respiratory chain (such as *L. lactis*), this gradient is maintained by the membrane-bound H<sup>+</sup>-ATPase, which hydrolyses ATP to actively pump protons out of the cytoplasm. This coupling of influx and pumping of protons to ATP synthesis and hydrolysis, respectively, not only maintains the cellular pH but also maintains the electrochemical and pH gradient required to drive many other cellular processes [52, 53].

Activity of the H<sup>+</sup>-ATPase has been found to increase when the cytoplasm becomes slightly acidic. It actively pumps protons out of the cytoplasm, driven by hydrolysis of ATP. Conversely, H<sup>+</sup>-ATPase activity has been found to decrease when the cytoplasm becomes more alkaline, using the passive influx of protons to phosphorylate ADP [51, 50]. This change in proton pumping, dependent on cytoplasmic conditions, is brought about by regulation of enzyme expression [54].

Hence, there are two ways to increase the activity of the H<sup>+</sup>-ATPase: 1) Over-expression of the *atp* gene, thereby increasing the concentration of H<sup>+</sup>-ATPase in the cytoplasmic

membrane [46], and 2) increased concentration of acid in the environment, which enters the cell via ion transporters and dissociates in the cytoplasm, dissipating the PMF and causing upregulation of H<sup>+</sup>-ATPase. Both these conditions would cause the cell to essentially disregard the availability of ATP and would enhance ATP hydrolysis in spite of the demand for ATP by other cellular processes, such as biomass production.

The question then arises as to how the glycolytic flux would respond to such an increased ATP demand. Koebmann *et al.* [55] showed in another model organism, *Escherichia coli*, that uncoupling ATPase activity from biomass production results in a nearly-doubled glycolytic flux, indicating that control over the glycolytic flux does not only reside with the activities of glycolytic enzymes, but also with the rate of ATP consumption. However, similar work in growing *L. lactis* cells showed no change in flux in response to an increase in ATP consumption [42]. How would these responses compare to other species with similar metabolic networks?

#### *1.4.4 Implications for this study*

Progress in microbiological research has led to the exploitation of bacterial antagonism in the improvement of industrial-level fermentation of most dairy products [12, 56]. The fermentation rate must be optimized to suit the preservative requirements. The rate at which *L. lactis* produces lactic acid (as well as other flavour components, such as diacetyl and acetoin) can be controlled by genetically modifying certain enzymes in the glycolytic pathway. In-depth knowledge of the control distribution of glycolysis between the various enzymes is therefore necessary, as well as a clear understanding of the metabolic fluxes and rates [21].

This study will contribute to the understanding of *in vivo* metabolism of the model organism, *Lactococcus lactis* ssp. *cremoris* by performing ATP supply-demand analysis in non-growing cells. Non-growing conditions were used in order to exclude the additional ATP demand represented by biomass production during cell growth, in order to focus on ion-pumping ATPases as consumers of ATP. The experimental data will be obtained by monitoring glucose metabolism – and resulting ATP/ADP ratios – by means

of nuclear magnetic resonance (NMR) spectroscopy. This analytical method was selected as it enables the *in vivo* analysis of organically-relevant nuclei in intact cells. The theory of nuclear magnetic resonance and its applications to biological systems are discussed in Section 1.5.

## 1.5 Nuclear magnetic resonance spectroscopy

### 1.5.1 Theory of NMR

#### 1.5.1.1 Spin

The concept of a magnetic spin moment of certain types of nuclei was first proposed in the 1920s [57]. Nuclei possess the physiochemical properties of mass (neutrons and protons), as well as charge (protons). On a physiochemical level, each of these nucleons continuously spins around its own axis. However, most nuclei have one or more isotopes that have odd (uneven) numbers of protons and/or neutrons, and such a nucleus possesses an intrinsic angular momentum. The overall angular momentum, or spin, is dependent on a quantified property, the spin quantum number ( $I$ ), expressed in integral or half-integral values [58].

$$\text{Spin} = \hbar \sqrt{I(I + 1)} \quad [\text{Eq. 17}]$$

The component  $\hbar$  is known as the reduced Planck's constant:  $\hbar = h/2\pi$ , where  $h$  = Planck's constant. Planck's constant quantifies the relationship between the frequency of an electromagnetic wave and its energy. In nuclei with an uneven number of protons and/or neutrons,  $I \neq 0$ .

#### 1.5.1.2 The gyromagnetic ratio

Any charged body spinning around an axis generates a magnetic field along that axis [59]. Therefore, nuclear spin ( $I \neq 0$ ) confers upon the nucleus a magnetic moment ( $\mu$ ), which is aligned either parallel or anti-parallel to the angular momentum [58, 59]. Each magnetically active nucleus is uniquely characterised by the ratio between its magnetic moment and angular momentum, known as the gyromagnetic (or magnetogyric) ratio [58]:

$$\gamma = \mu/I(2\pi/\hbar) = \mu/\hbar I \quad [\text{Eq. 18}]$$

The value of the gyromagnetic ratio is positive or negative depending on whether the magnetic moment and angular momentum are parallel or anti-parallel vectors, respectively.

A nucleus with  $I \neq 0$  can assume more than one spin state, depending on the energy state of the nucleus. The number of spin states a nucleus can assume equals  $2I + 1$ , which in the presence of an externally applied static magnetic field ( $B_0$ ) translates into  $2I + 1$  potential orientations the nucleus can assume with respect to  $B_0$ . Therefore, a nucleus with  $I = \frac{1}{2}$  can assume  $2(\frac{1}{2}) + 1 = 2$  orientations, one being aligned with  $B_0$  ( $m = +\frac{1}{2}$ ) and one aligned against  $B_0$  ( $m = -\frac{1}{2}$ ). A nucleus in the presence of a magnetic field will assume the more energetically favourable, and therefore more stable, orientation of  $m = +\frac{1}{2}$  (aligned with the magnetic field), unless energy is applied to induce it to assume the less stable (higher energy) orientation  $m = -\frac{1}{2}$  (against the field) [59].

### 1.5.1.3 Precession

The alignment of spinning nucleus to the magnetic field  $B_0$  is not two-dimensional, due to the angular momentum of the nucleus. With the direction of  $B_0$  along the z-axis, the nucleus oscillates (or precesses) in the xy-plane at an angle to the z-axis, the angle being either in the  $m = +\frac{1}{2}$  or  $m = -\frac{1}{2}$  direction. This can be diagrammatically represented as a three-dimensional cartesian system with two precession cones, one angled in the direction of the magnetic field and the other in the opposite direction (see Figure 1.5).

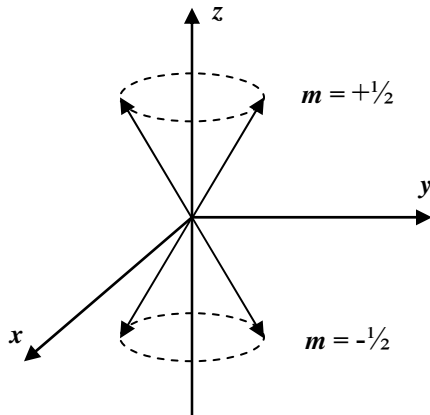


Figure 1.5. A magnetically active nucleus precesses around the  $z$ -axis either aligned with or against the applied magnetic field  $B_0$ . Magnetisation is in the direction of the  $z$ -axis and magnetisation along the  $xy$ -plane is zero [60].

With one orientation being more energetically favourable than the other, it would require a certain minimum amount of energy to induce the transition from one energy state to another (e.g. to the less energetically favourable orientation). Application of an external, oscillating magnetic field ( $B_1$ ), perpendicular to  $B_0$  and with a frequency  $\nu_0$ , can provide sufficient energy to induce this transition. The energy required is proportional to the gyromagnetic ratio of the nucleus and the static applied magnetic field  $B_0$  in which the nucleus finds itself [60].

$$\Delta E = \gamma \hbar B_0 \quad (\Delta E = \text{the energy difference between the orientations}) \quad [\text{Eq. 19}]$$

The energy of the applied oscillating field  $B_1$  is proportional to the frequency of the oscillating field  $\nu$  [60]:

$$\Delta E = h\nu_0 \quad [\text{Eq. 20}]$$

The above equations demonstrate the proportionality between the energy difference between the two states and the frequency of the applied magnetic field which is required

to bridge that energy difference. From these equations, the value of  $\nu_0$  can be defined as follows [60]:

$$\nu_0 = B_0(\gamma/2\pi) \quad [\text{Eq. 21}]$$

The variable  $\gamma$ , which is characteristic for each type of nucleus, therefore also bestows upon each type of nucleus a characteristic magnetic field frequency ( $\nu_0$ ) which would induce the transition to a less energetically favourable state.

#### 1.5.1.4 Secondary magnetic field ( $B_{\text{eff}}$ )

The electrons of an atom respond to the static magnetic field  $B_0$ , generating a miniscule electric current which results in a secondary magnetic field. The magnitude of this field is dependent on the nature of neighbouring nuclei and the level of covalency between the electrons. For a specific nucleus type, surrounded by certain atoms with specified types of inter-atomic bonds, a proportionality constant  $\sigma$  (known as the “shielding constant”, see Section 1.5.2.2) applies to the secondary electromagnetic interactions between the electrons of a nucleus and the electrons of its neighbouring nuclei, which, combined with the applied field  $B_0$ , give the magnitude of the total effective magnetic field,  $B_{\text{eff}}$  [60]:

$$B_{\text{eff}} = B_0(1 - \sigma) \quad [\text{Eq. 22}]$$

With  $B_{\text{eff}}$  now becoming the total magnetic field influencing different orientations of the spinning nucleus, the  $B_1$  frequency ( $\nu_0$ ) would now be redefined as:

$$\nu_0 = B_0(1 - \sigma)(\gamma/2\pi) \quad [\text{Eq. 23}]$$

From this equation it can be deduced that the radiofrequency which excited a nucleus is determined by the nature of the nucleus itself (indicated by  $\gamma$ ), as well as the natures of the neighbouring nuclei and the interactions between them (indicated by  $\sigma$ ) [60].



### 1.5.1.5 Angular frequency ( $\omega$ )

A nucleus spins around the z-axis with an angular momentum and the frequency at which it does so is described by the term *angular frequency* ( $\omega_0$ ). This angular frequency (known as the Larmor frequency) is a function of the gyromagnetic ratio of the nucleus and the magnitude of the static magnetic field  $B_0$ , as described by the Larmor equation [60, 61]:

$$\omega = \gamma(B_0) \quad [\text{Eq. 24}]$$

The Larmor frequency relates to the energy of the required exciting magnetic field by means of the reduced Planck's constant ( $\hbar$ ):

$$\Delta E = \hbar \cdot \omega \quad [\text{Eq. 25}]$$

This relationship represents the ratio between energy and the frequency of its related electromagnetic field in radians per second. In order to excite a nucleus (and cause it to change orientation) the energy of the applied field  $B_1$  must equal the energy of the precessing nucleus within the static field  $B_0$ .

### 1.5.1.6 Relaxation

The application of a  $90^\circ$  oscillating magnetic field  $B_1$  induces the magnetisation of a nucleus to align itself in the  $m = -1/2$  (higher energy state) orientation and precess in the xy-plane (with respect to  $B_0$ ). The removal of  $B_1$  would leave the nucleus to swing back into  $m = +1/2$  (lower energy state) orientation and precess along the z-axis (parallel to  $B_0$ ). This equilibration of the nucleus into a more stable alignment of magnetisation along the z-axis is known *relaxation* and involves an energy exchange between the nucleus and its electrochemical environment. [55, 60].

Relaxation of a nucleus consists of two major processes: 1) restoration of magnetisation ( $M_z$ ) along the z-axis (parallel to  $B_0$ ), and 2) time-dependent decay of magnetisation ( $M_{xy}$ ) in the xy-plane. Although these two processes theoretically take place simultaneously,

they do not necessarily require the same amount of time to completion. These two processes are each therefore characterised by different time-constants: restoration of  $M_z$  to its pre-pulse value (otherwise known as spin-lattice relaxation) is allocated the time constant  $T_1$  and decay of  $M_{xy}$  to its pre-pulse value of 0 (known as spin-spin relaxation) is allocated the time constant  $T_2$ . While the spin-lattice relaxation process involves an exchange of energy with the electrochemical environment (the lattice), spin-spin relaxation is only affected by interactions between neighbouring spinning (magnetically-active) nuclei [60].

It is this resonance or decay of magnetization in the xy-plane ( $M_{xy}$ ), following a  $B_1$  pulse, which is detected as a signal by the radiofrequency coil of the resonance spectrometer and known as the free induction decay (FID).

### *1.5.2 Practical NMR spectroscopy*

#### 1.5.2.1 Fourier transform

For the purposes of NMR spectroscopy, the nuclei in a homogenous or non-homogenous mixture need to be excited. For a perfectly homogenous mixture of a nucleus type, a  $90^\circ$  pulse at only one frequency (the  $\nu_0$  characteristic to that nucleus) is required. However, for a non-homogenous mixture of nuclei, the radiofrequency (RF) pulse must be set to cover a range of frequencies, thereby exciting nuclei in different chemical environments. The RF pulse originates from the spectrometer's transmitter coil, which is set to a certain bandwidth, or range of frequencies covered by a single pulse. All the decaying resonances of all the nuclei within the RF pulse range are detected simultaneously during the delay before the next pulse [60].

The raw signal detected by the spectrometer is displayed as a decaying oscillation, a sinusoidal wave with decaying amplitude (the free induction decay, FID) [58, 60]. It is composed of the decaying resonance signals of all the excited nuclei in one complex bundle. For visualisation purposes, raw FID data are subjected to Fourier transformation – a mathematical conversion from time-dependent decay signal to a frequency spectrum on which nuclei with different resonating frequencies are distinguishable as peaks, the

area of which is proportional to the number of nuclei contributing to their signal (see Figure 1.6).

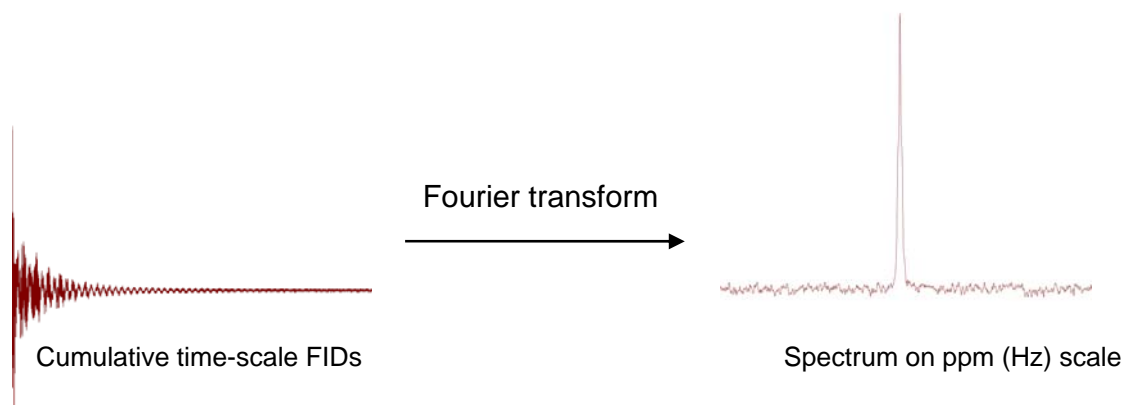


Figure 1.6. Original cumulative FIDs showing decaying resonance on a time scale, processed by Fourier transform to produce a Hz-scale spectrum of peaks representing nuclei excited at different frequencies (chemical shift).

Modern NMR spectrometer software includes programs which automatically perform the Fourier transformation calculations and yield a frequency scale showing peaks at their various chemical shifts. However, stand-alone programs are also available which can use raw FID data to yield frequency scale spectra, e.g.:

ACD Labs (<http://www.acdlabs.com>)

VNMR (<http://www.varianinc.com>)

MestreNova (<http://mestrelab.com>)

#### 1.5.2.2 Chemical shift

As previously described, the frequency of field  $B_1$  which would excite a particular nucleus is a function of the gyromagnetic ratio ( $\gamma$ ) and the static magnetic field ( $B_0$ ), since it must match the angular frequency at which the nucleus precesses. However, the electrons surrounding the protons of neighbouring nuclei interact electromagnetically with the electrons surrounding the proton of the nucleus being studied, and these cause it not only to respond slightly differently to the static field  $B_0$  (i.e. cause it to have a

different precession energy), but also thereby cause it to respond to a slightly different frequency of pulse  $B_1$ . This phenomenon, known as “shielding”, causes nuclei of the same type – but with different bond types between themselves and different neighbouring nuclei – to resonate in response to slightly different pulse frequencies [60]. For this reason, an RF pulse applied for the purpose of exciting nuclei would pulse over a relatively small range of frequencies (band-width) in order to excite all nuclei of the same species within the required range. The deviation of the response of nuclei from a reference frequency is referred to as the *chemical shift* [60, 61]. The differences in resonance frequencies between different species of nuclei are usually on a MHz scale, whereas the chemical shift between nuclei of the same type is on a Hz scale. The FID obtained from each pulse is Fourier-transformed into a ppm (or  $\delta$ ) scale, which represents a Hz/MHz-scale (this conversion also standardises the scale to be comparable between various instruments, which have different strength magnets and consequently different resonance frequencies for a particular nuclide). The  $\delta$  scale is derived from the fractional difference between the resonance frequency ( $\nu_i$ ) of a nucleus and the resonance frequency of a reference nucleus ( $\nu_{\text{ref}}$ ) [61]. On this ppm scale, nuclei in different chemical environments (i.e. with different levels of interaction between their electrons and those of neighbouring atoms) can sometimes be distinguished clearly from one-another and sometimes less so, depending on differences in the strength of the “shielding” [60].

### 1.5.2.3 Peak splitting

The electrons of a population of magnetically-identical nuclei interact to different extents with the total effective field  $B_{\text{eff}}$  and this results in some nuclei even in the same chemical environment to resonate at minutely different frequencies from others in the population. The interaction between decaying magnetizations ( $M_{xy}$ ) of magnetically active nuclei causes *spin-spin coupling* between neighbouring nuclei [58, 60]. Each nucleus forms its own secondary magnetic field in response to a RF pulse, shielded to some extent by neighbouring nuclei (Section 1.5.1.4). As a result, a population of nuclei will divide into groups representing nuclei which are shielded by neighbouring nuclei and nuclei which are not. Furthermore, if neighboured by more than one type of nucleus, a further group emerges which is shielded to a different extent by this type of nucleus.

These groups of a population are detectable as peaks in a spectrum which are split into sub-peaks, with a segment of the population of nuclei tending to resonate at a minutely different frequency than the rest of the population(s). The number of sub-peaks and their sharpness is determined by the number of neighbouring resonating nuclei affecting the magnetization of the original nucleus population, as well as the strength of the electromagnetic interactions between such neighbouring nuclei.

When using peak areas to deduce the number of nuclei of a certain type and electrochemical nature, summation of all the peak areas originating from the nucleus in question is required in order to include all groups belonging to the same population. Therefore, if a peak splits into two or three secondary peaks according to its chemical environment and the interactions described above, it is necessary to sum the areas of all the secondary peaks in order to get a value proportional to the actual number of nuclei of that specific type.

#### 1.5.2.3 Experimental $T_1/T_2$ calibrations

Immediately following excitation by an electromagnetic pulse, certain nuclei take longer to restore their equilibrium magnetization ( $M_z$ ). If resonating nuclei are not fully relaxed before the next pulse is applied, an incomplete free induction decay (FID) is detected and the resulting signal is weaker than it would be if all nuclei were allowed to fully relax before being excited by the next pulse. This incomplete signal detection would result in an inaccurate estimate of the number of nuclei present, since the entire  $M_{xy}$  decay process is not detected.

However, if the delay between pulses is set to the maximum possible  $T_1$  and  $T_2$  required for all nuclei to be fully relaxed, the time required for an experiment consisting of sufficient cumulative FID's would be unfeasible. For example, if the relaxation delay was increased from one second to 10 s, the resulting experiment would take four hours as opposed to 24 min. It would be impossible to complete batch experiments of five or more samples in a single day - cells in buffer would become starved during the course of the

experiment and biological material in the sample would begin to degrade after some time, rendering the quantifications taken later in the course of the experiment less accurate than those taken earlier.

It is not desirable to reduce time required per experiment by decreasing the number of FIDs – since the intensity of the signal depends on the number of cumulative FIDs acquired, reducing the number would reduce the ratio between signal intensity and background “noise” [60].

This obstacle can be addressed by performing a  $T_1/T_2$  experiment, whereby the number of scans is maintained, but the relaxation delay is set alternately to one second and then to a longer time delay (e.g. 10 s). A calibration value can be determined from the difference in peak areas and each peak can be calibrated for this difference resulting from insufficient relaxation time.

With the above theory and background in mind, the following section will describe the application of NMR spectroscopy (initially a technique based on chemical applications) to studying biological systems and molecules.

### *1.5.3 Biological applications of NMR spectroscopy*

NMR spectroscopy has evolved over the last 70 years from a mere interesting phenomenon to a powerful analytical tool with a vast range of chemical and biological applications [57, 62].

The 1970s saw the extension of NMR applications to studies of whole cells and intact tissues. NMR techniques were adapted to non-invasive, in vivo detection of compounds containing resonating isotopes, such as  $^1\text{H}$ ,  $^{13}\text{C}$  and  $^{31}\text{P}$ . This adaptation (analysis of intact, living cells and tissues) made NMR unique as an analytical method and was the basis for current MRI (magnetic resonance imaging) diagnostic techniques used in medical examination of tissues, organs and other localized body regions, as it enables the

detection of molecules containing hydrogen, carbon or phosphorus nuclei in the cellular milieu.

Proton NMR ( $^1\text{H}$ ) has the advantage of having the highest resolution and signal-to-noise ratio of all isotopic nuclei. The disadvantage of using  $^1\text{H}$  to detect compounds in living cells and tissue is that most tissues contain large amounts of water. The high  $^1\text{H}$  signal detectable from water may overshadow the less intense signals of the small amounts of  $^1\text{H}$  in other compounds.

In relation to  $^1\text{H}$ , the  $^{13}\text{C}$  nucleus not only gives off a weak signal during NMR, but also has a low natural abundance (1.1 %) [62]. This means that enrichment is necessary with either a very high concentration of unlabelled carbon source (1.1%  $^{13}\text{C}$ ) or a source rich in  $^{13}\text{C}$  (labelled) [60]. A theoretical advantage of the low natural abundance of  $^{13}\text{C}$  for the purposes of metabolic NMR studies is that carbon metabolism can be more accurately and less ambiguously monitored upon  $^{13}\text{C}$ -enrichment, since most of the detectable carbon stems from the experimentally-added carbon and not the existing intracellular carbon [60].

Metabolic studies, such as that conducted by Neves *et al.* [63], are reliant on  $^{31}\text{P}$  NMR for the purpose of detecting phosphorous-containing energy metabolites such as ATP, ADP, AMP, phosphocreatine and inorganic phosphate. Unlike  $^{13}\text{C}$ ,  $^{31}\text{P}$  has a natural abundance of nearly 100 % [60, 64]. While not as sensitive as  $^1\text{H}$ ,  $^{31}\text{P}$  NMR does have two advantages over  $^{13}\text{C}$  NMR: 1) all phosphate-containing compounds being detected are from intracellular pools, since immobilised (e.g. membrane bound) phosphate-containing molecules are virtually undetectable with NMR spectroscopy [60], and 2) the high natural abundance of  $^{31}\text{P}$  means that enrichment with a  $^{31}\text{P}$ -source is not necessary for NMR analysis, since cellular  $^{31}\text{P}$  is normally sufficient for studies of energy metabolism and intracellular pH. Different phosphorous molecules comprising cellular energy metabolites can be detected separately: for example the  $\beta$ - $^{31}\text{P}$  of ATP, flanked by two phosphate bonds, would resonate at a slightly different frequency to the  $^{31}\text{P}$  nucleus of an inorganic phosphate molecule. This feature of  $^{31}\text{P}$  NMR will be exploited to determine the ratio of

ATP/ADP in mixtures of live cells and/or in cell-free extracts, in order to determine the energy state of the cells at different times and under different conditions.

This chapter has described the physiology and metabolism of the model organism MG1363, the theory of supply-demand analysis (which will be applied to studying the metabolism of MG1363) and the technique,  $^{13}\text{C}$  and  $^{31}\text{P}$  FT-NMR, by which metabolic data will be acquired under various conditions.

### **1.6 Aims and outline of this thesis**

The aim of this study is to apply the principles of supply-demand analysis to experimental data in order to investigate the distribution of control of anaerobic free-energy metabolism, in non-growing *Lactococcus lactis* under conditions of glucose excess, between the energy supply (glycolytic flux) and energy demand (ATP consuming) pathways.

Chapter 2 serves to describe validation methods applied to raw data in the form of standardisations and calibration. Experimental results and preliminary supply-demand analysis data are presented in Chapter 3 and these results are discussed and contextualised in Chapter 4. Experimental procedures are described in Chapter 5, including all materials, methods and calculations employed.



## CHAPTER 2: STANDARDS AND CALIBRATIONS

As outlined in Section 1.5.2.3, data acquired by means of rapidly pulsed  $^{13}\text{C}$  and  $^{31}\text{P}$  NMR spectroscopy had to be validated by means of qualitative standards and had to undergo quantitative calibrations. This chapter serves to describe all standards used for qualification and quantification of acquired data, as well as all calibrations applied.

### 2.1 Growth rates of *L.lactis* strains

Cells were grown as described in Chapter 5 and their growth was monitored in terms of optical density, or quantifiable light absorption at a specified wavelength. For each *L.lactis* strain, MRS broth (100 ml) was inoculated with 1 ml of pre-culture, and spectrophotometric readings (Jenway 6100 spectrophotometer,  $\lambda = 600\text{ nm}$ ) were taken at  $t_0$  and repeated at 60-minute intervals (during the initial phase), which was reduced to 30-minute intervals (during exponential growth phase). A growth curve (Figure 2.1) was compiled for each strain, which was used to predict the growth rate in exponential growth phase.

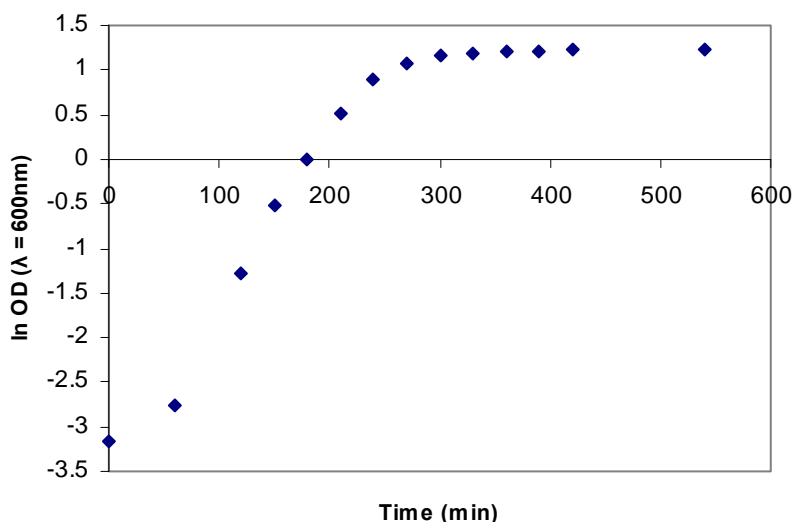


Figure 2.1. Growth of *L.lactis* spp *cremoris* strain MG1363 in MRS broth at  $30\text{ }^{\circ}\text{C}$ , monitored as spectrophotometric turbidity at  $\lambda = 600\text{ nm}$ .

An initial lag phase was observed, after which exponential growth phase occurred between  $t = 180$  and  $t = 240$  minutes. From approximately  $t = 270$  minutes (and  $OD \approx 3.00$ ) cells began to enter stationary phase, during which little or no growth occurred.

During exponential growth phase, the increase in turbidity over time was used to calculate the specific growth rate ( $\mu$ ) via the following equation:

$$\ln(x / x_0) = \mu \cdot (t - t_0) \quad [\text{Eq. 26}]$$

In the above equation,  $x_0$  is the initial turbidity, or optical density, at  $t_0$  ( $t = 180$  min) of the exponential growth phase and  $x$  is the turbidity at  $t$  ( $t = 240$  min) of exponential growth phase. The doubling time ( $t_D$ ) was calculated by adapting the equation as follows:

$$\ln(2x_0 / x_0) = \mu \cdot (t_D)$$

Therefore:

$$t_D = \ln 2 / \mu \quad [\text{Eq. 27}]$$

The specific growth rates and doubling times of exponential-phase cells, for the three strains of *L.lactis* ssp *cremoris* utilised in this study, are shown in Table 2.1. These growth rates enabled coordination of cell harvesting (for experimental applications) with exponential growth phase of the cells.

Table 2.1. Growth rates and doubling times of three *L.lactis* ssp *cremoris* strains during exponential growth phase.

<i>L.lactis</i> strain	Exponential growth rate constant, $\mu$ ( $\text{h}^{-1}$ )	Doubling time (min)
MG1363 [65]	0.91	45.7
CS 8 [10]	0.70	59.4
BK1506 [46]	0.64	65.0

## 2.2 Dry weight

The amount of metabolically-active cellular material in a suspension can be determined by measuring the dry weight of the total sample or the optical density of the sample in suspension. Dry weight is a more accurate measurement of cellular material, while optical density (OD) of suspensions is much quicker and more convenient to measure by spectrophotometric means. However spectrophotometric measurement of OD is dependent on the quantification of light-scattering – the dispersion of light by cellular material in suspension – which varies between different instruments. Since OD is more convenient to measure than dry weight of cellular material, the relationship of OD to dry weight was determined (Figure 2.2) for the spectrophotometer used (see Chapter 5). Cell suspensions in deionized water were measured for OD, after which 1 ml of cell suspension was passed through a 0.2  $\mu\text{m}$  filter, retaining all cellular material. This filtered biological material was dried and weighed (normalising to the mass of the filter).

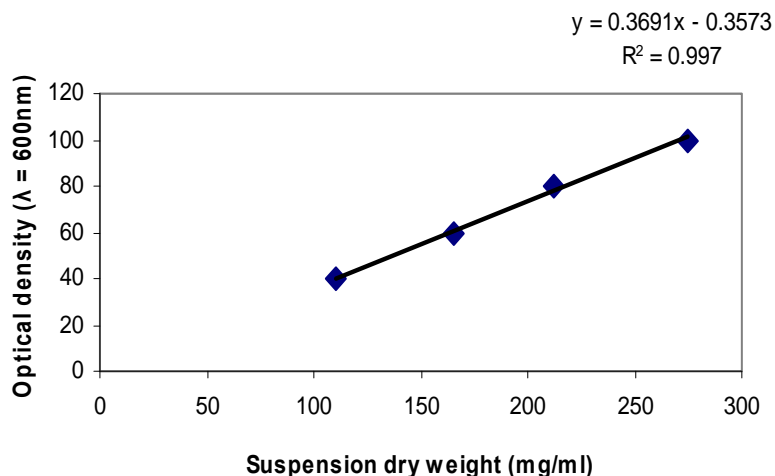


Figure 2.2. Dry weight of total cell suspensions with a range of spectrophotometrically-measured optical densities.

## 2.3 NMR standards

### 2.3.1 $^{13}\text{C}$ NMR: Glucose standards

The internal standard used for  $^{13}\text{C}$  spectroscopy was 2-(N-morpholino)ethanesulfonic acid (MES), which has four distinct types of carbon nuclei. Glucose standards were prepared as follows: a suspension of stationary-phase cells (OD 60-80) in 500 mM MES buffer and 10 %  $\text{D}_2\text{O}$  was spiked with uniformly  $^{13}\text{C}$ -labelled glucose and analysed at 30 °C on a Varian Unity Inova NMR spectrometer at 150.8 MHz. For this qualitative assignment of peaks, the chemical environment of the standards was the same as that of experimental samples. The resulting spectrum is shown in Figure 2.3 – a good example of how even anomeric forms of the same carbon atoms display different chemical shifts. The internal standard, MES, has six structural carbons of which two pairs are identical in their chemical environments and thus resonate at the same frequency. Therefore, MES only produces four discernable peaks on a Fourier transformed spectrum.

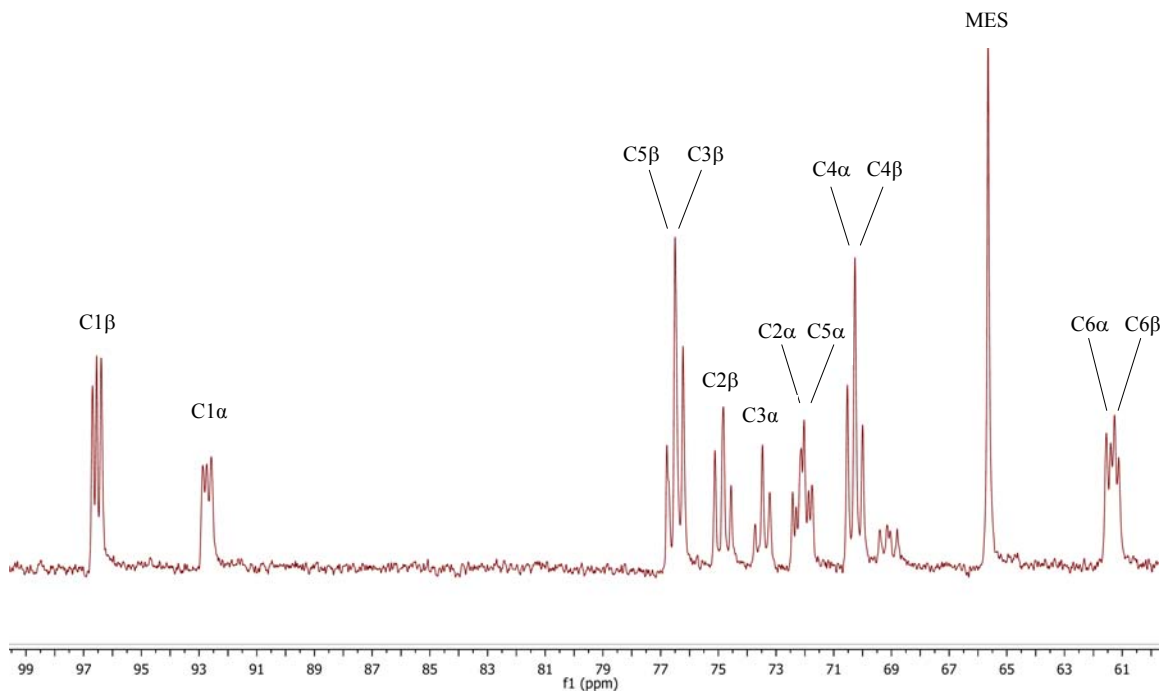


Figure 2.3. Uniformly  $^{13}\text{C}$ -labelled glucose was added to stationary-phase cells and analysed at 150.8 MHz on a 600 MHz spectrometer for 71 FIDs, with the following parameters: pulse width = 3.1  $\mu\text{s}$ , acquisition time = 0.7 s and relaxation delay = 1 s. Carbons 1-6 are shown, as well as their  $\alpha$ - and  $\beta$ -anomers, in relation to the internal standard, 2-(N-morpholino)ethanesulfonic acid (MES). MES yields four distinguishable peaks (at 65.65 ppm, 56.65 ppm, 53.27 ppm and 46.64 ppm), of which only one is shown here in order to expand the spectrum for better resolution.

In the spectrum shown in Figure 2.3, certain peaks appear as split into two (known as doublets) or three (known as triplets). As described in Chapter 1, electromagnetic (spin-spin) coupling occurs between any two neighbouring spinning nuclei: the electron cloud surrounding a nucleus interacts slightly with the neighbouring nuclei and their electron clouds. The nucleus is somewhat shielded from the effect of an applied electromagnetic pulse by these neighbouring nuclei, thereby causing it to respond to a slightly higher or lower pulse frequency, thereby separating one peak into two or more populations of nuclei, depending on which neighbouring nucleus they interact the most strongly with. The number of split peaks depends on the number and types of magnetically active nuclei

flanking the nucleus of interest, represented by a certain peak. The nuclei composing a single peak are divided equally between the different orientations, some interacting more or less with the neighbouring nuclei, hence the chemical shift of the nuclei interacting more strongly with one neighbouring nucleus will be fractionally different from that of the nuclei either interacting more strongly with another neighbouring nucleus, or not interacting with any neighbouring nuclei [60].

Furthermore, if the same carbons of different anomers differ significantly in chemical environment, they will demonstrate quite different resonance frequencies. For example, the difference in chemical conformation between the  $\alpha$  and  $\beta$  isoforms of glucose causes the C1 anomers to have slightly different resonance frequencies. Furthermore, the C1 of glucose has two neighbouring carbons and each C1 anomer will therefore appear as a triplet. Interaction with the magnetic fields of other species of nuclei, e.g.  $^1\text{H}$  or  $^{31}\text{P}$ , results in very noticeable chemical shifts (separated by several ppm), whereas shielding by neighbouring carbons has a lesser effect and is only noticeable as peak splitting.

### 2.3.2 $^{31}\text{P}$ NMR: ATP and ADP standards

#### 2.3.2.1 Inorganic (cell-free) standards

Solid ADP and ATP were dissolved in 15 %  $\text{D}_2\text{O}$ , with 30 mM sodium-EDTA (pH 8.2) and 1 mM triethyl phosphate (TEP) as internal standard [66]. The standards were analysed for three hours at 161.9 MHz in a 400 MHz Varian spectrometer, with the following parameters: pulse width = 3.1  $\mu\text{s}$ , relaxation delay = 1 s, acquisition time = 1.6 s, spectral width of -60 ppm to 60 ppm (Figures 2.4 and 2.5).

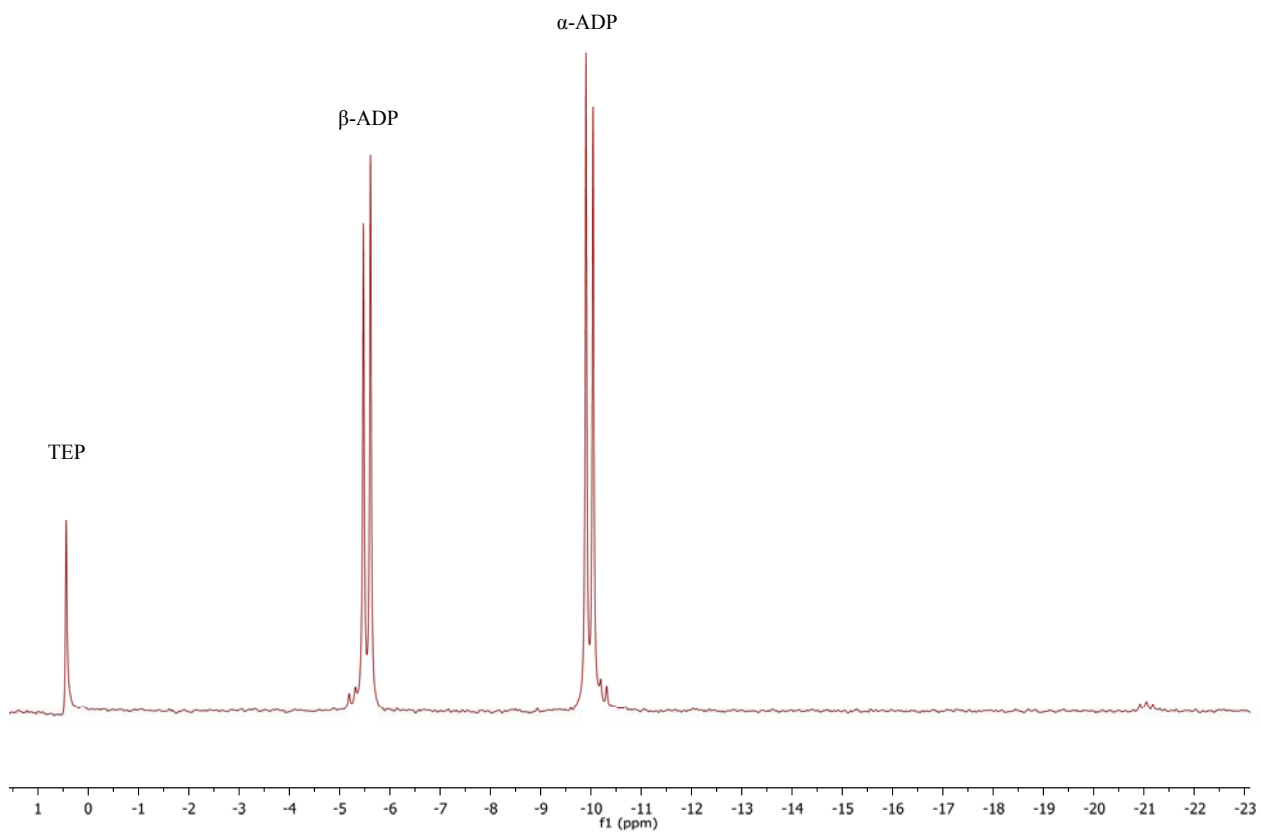


Figure 2.4. Standard solution of 10 mM ADP in 15 % D<sub>2</sub>O and 30mM EDTA (pH 8.2). Standards were analysed for three hours at 161.9 MHz on a 400 MHz Varian NMR spectrometer. TEP (1 mM) was used as an internal reference ( $\delta = 0.44$  ppm).

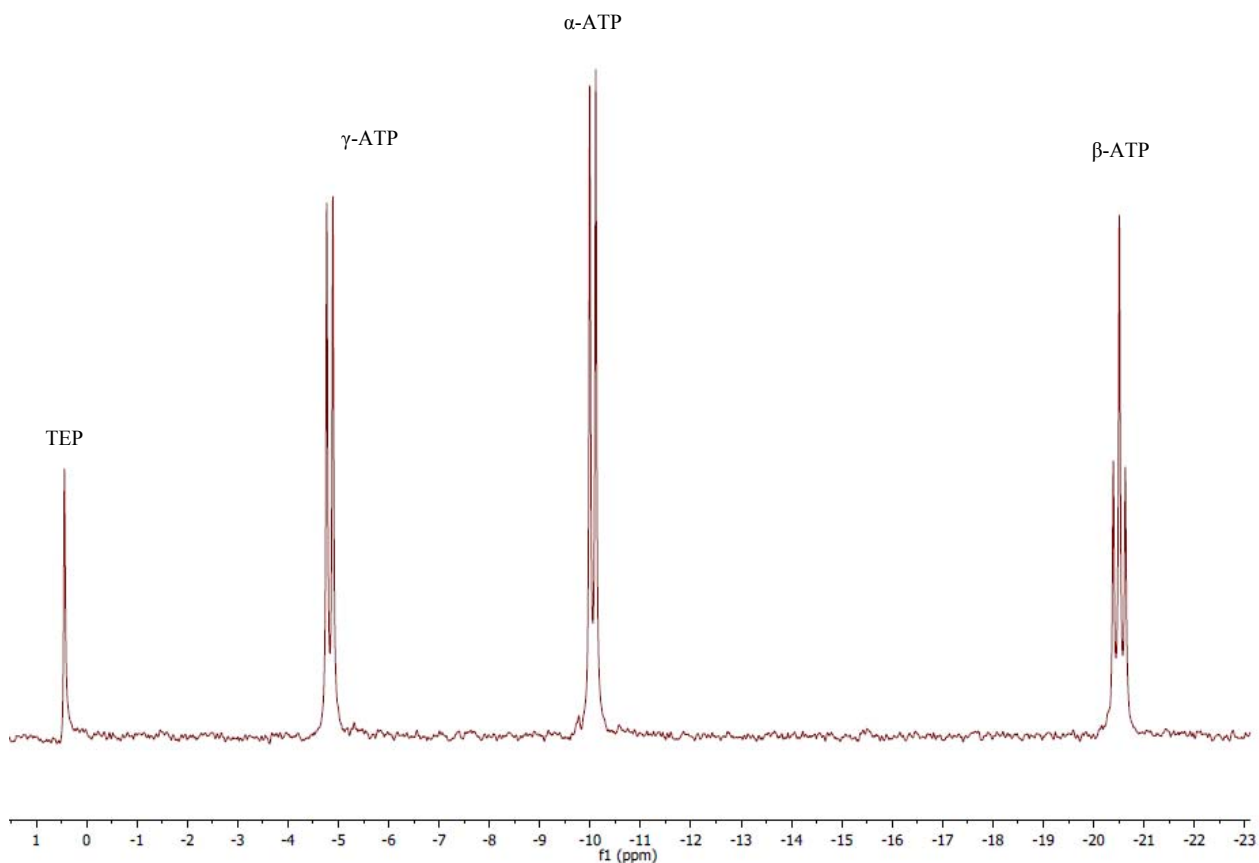


Figure 2.5. Standard solution of 10 mM ATP in 15 % D<sub>2</sub>O and 30mM EDTA (pH 8.2). Standards were analysed for three hours at 161.9 MHz on a 400 MHz Varian NMR spectrometer. TEP (1 mM) was used as an internal reference.

The  $\beta$ -<sup>31</sup>P peak of ADP was detected at -5.7ppm to -5.9ppm, and the  $\alpha$ -<sup>31</sup>P peak of ADP at -9.9 ppm to -10.1 ppm. The  $\gamma$ -<sup>31</sup>P peak of ATP demonstrated a chemical shift of -4.6 ppm to -5.0 ppm, the  $\alpha$ -<sup>31</sup>P peak of ATP at -9.8 ppm to -10.2 ppm and the  $\beta$ -<sup>31</sup>P peak of ATP at -20.4 ppm to -20.8 ppm. The spectrum was calibrated with TEP (internal standard) at 0.44ppm.

As previously described (Section 2.3), spin-spin coupling occurs between neighbouring magnetically-active nuclei and spectral peaks can appear split into doublets or triplets depending on the number of such neighbouring nuclei. The  $\alpha$ -<sup>31</sup>P and  $\gamma$ -<sup>31</sup>P of ATP each only have one neighbouring <sup>31</sup>P nucleus and therefore appear as doublets as they are



shielded only by one neighbouring phosphorous nucleus. The  $\beta$ - $^{31}\text{P}$  of ATP is flanked by two  $^{31}\text{P}$  nuclei and therefore appears as a triplet peak.

As can be seen by comparing the chemical shifts,  $\alpha$ -ADP and  $\alpha$ -ATP, as well as  $\beta$ -ADP and  $\gamma$ -ATP, did not resolve very clearly from one another, which would make integration of these peaks in a mixture more difficult. Furthermore, ADP and ATP peak resonances will differ between an inorganic solution and a cell extract sample, depending on factors such as pH and other solutes. In order to be able to accurately identify ADP and ATP in a typical sample environment, it is necessary to mimic the chemical environment of the typical sample and determine which peaks change in intensity after spiking with pure standard (ADP or ATP).

#### 2.3.2.2 Sample environment standards

The phosphorous nuclei of ADP and ATP demonstrate different resonances (or chemical shifts) in different chemical environments, such as different pH. In order to identify ADP and ATP peaks in an environment identical to a typical sample, an extract of intracellular phosphate metabolites was prepared, as described in Materials and Methods (Chapter 5). The cell extract was then manually spiked with excess ADP and/or ATP, in order to determine the spectral pattern of these phosphate peaks in the sample environment (Figure 2.6). The pH of each sample was checked after analysis to ensure constant conditions.

TEP

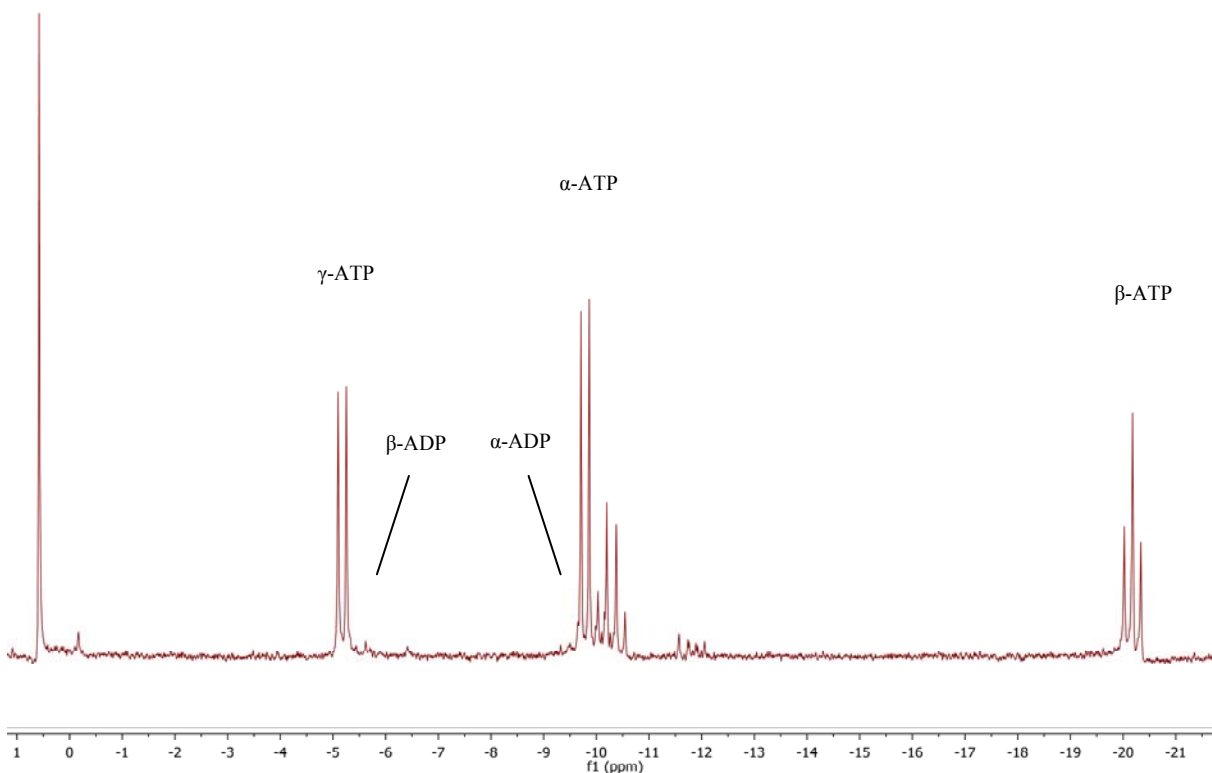


Figure 2.6. An extract of intracellular metabolites was prepared (as described in Section 5.3.1), freeze-dried and resuspended in 15% D<sub>2</sub>O and 30 mM EDTA (pH 8.2) [78]. ATP (1mM) was added to the resuspended sample, which was then analysed at 161.9 MHz on a Varian 400MHz spectrometer for 19300 FIDs, with the following parameters: pulse width = 3.1  $\mu$ sec, acquisition time = 1.6 sec, relaxation delay = 1 sec.

## 2.4 Relaxation-time calibrations

### 2.4.1 <sup>13</sup>C relaxation delay calibrations

Not all nuclei require the same length of time return to a fully relaxed state ( $T_1$ ). Quantitative analysis of rapidly pulsed spectra requires calibration with fully relaxed spectra (Section 1.5.2.3). Due to the high number of FIDs required to attain a good signal-to-noise ratio, it was not feasible in terms of time to lengthen the delay between pulses. However, a short delay between pulses would result in an inaccurate representation of the number of molecules detected, as not all molecules would have fully relaxed between pulses. Samples were therefore rapidly-pulsed and a  $T_1$  experiment was

performed in which the ratios between peak areas in fully-relaxed and rapidly-pulsed spectra were used to determine correction factors with which rapidly-pulsed spectra were calibrated to represent fully-relaxed peak areas.

A cell suspension was prepared as in prior experiments (described in Chapter 5) and analysed at 150.8 MHz on a Varian 600 MHz spectrometer for 36 FIDs per data point, with the following parameters: pulse width = 3.1  $\mu$ s, acquisition time = 0.7 s, relaxation delay = 1 s. The same sample was then analysed on the same instrument for 36 FIDs per data point, with the following parameters: pulse width = 3.1  $\mu$ sec, acquisition time = 0.7 sec, relaxation delay = 10 s. These experiments were repeated in an alternating pattern and a calibration curve was constructed for each  $^{13}\text{C}$  nucleus (Figure 2.8), with which all experimental results were calibrated before executing further analysis. Carbons 2 $\beta$  (Figure 2.7A) and 3 $\alpha$  (Figure 2.7B) showed marked differences in signal intensities between the partially and fully relaxed parameters, indicating they required calibration in order to estimate accurate levels of these nuclei. The correction factors for all carbon nuclei are shown in Table 2.2.

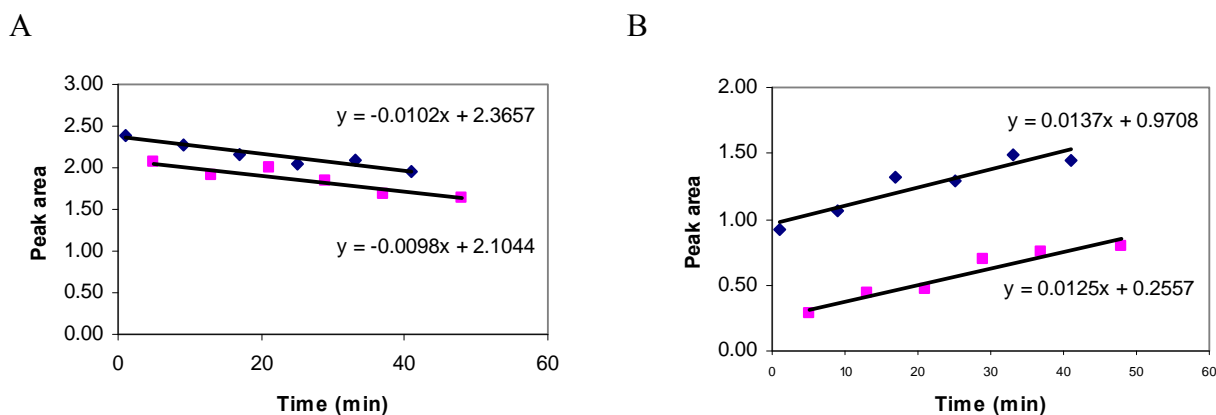


Figure 2.7. Relaxation calibration experiment for (A) glucose carbons 6 $\alpha$  and 6 $\beta$  and (B) lactate carbon 3, demonstrating differences in signal intensities between rapidly pulsed (relaxation delay = 1 s, blue) and fully relaxed (relaxation delay = 10 s, magenta) samples.

Table 2.2. Correction factors applied to data obtained from quantified  $^{13}\text{C}$  NMR signals to calibrate for incomplete relaxation of nuclei under experimental conditions.

$^{13}\text{C}$ nucleus	% unrelaxed/fully relaxed	Correction factor
Glucose C1 $\alpha$	100.00	1.000
Glucose C1 $\beta$	77.28	1.294
Glucose C2 $\alpha$ + C5 $\alpha$	96.62	1.035
Glucose C2 $\beta$	93.28	1.072
Glucose C3 $\alpha$	93.72	1.067
Glucose C3 $\beta$ + C5 $\beta$	90.17	1.109
Glucose C4 $\alpha$ + C4 $\beta$	94.25	1.061
Glucose C6 $\alpha$ + C6 $\beta$	87.49	1.143
Lactate C1	22.90	4.367
Lactate C2	53.56	1.867
Lactate C3	38.15	2.621

The correction factors for signal intensities obtained with relaxation times of 1 s and 10 s can be used to calibrate experimental values determined for all  $^{13}\text{C}$  nuclei.

#### 2.4.2 $^{31}\text{P}$ relaxation delay calibrations

During technical optimisation performed for this study, cell-free extracts from *L. lactis* consistently yielded low signal for intracellular  $^{31}\text{P}$ , which were detectable only from 19300 accumulated FIDs. A lower number of FIDs per spectrum would potentially give a poor resolution of  $^{31}\text{P}$  peaks, discouraging the reduction of the number of FIDs per spectrum. As with  $^{13}\text{C}$ , a good signal-to-noise ratio required a high number of FIDs and therefore a short delay between pulses.

An extract of intracellular phosphate metabolites was prepared, as described in Chapter 5. The sample was analysed at 161.9 MHz on a Varian 400 MHz spectrometer for 9650 FIDs, with the following parameters: pulse width = 3.1  $\mu\text{s}$ , acquisition time = 1.6 s, relaxation delay = 1 s. The same sample was then run on the same instrument for 9650

FIDs with the following parameters: pulse width = 3.1  $\mu$ s, acquisition time = 1.6 s, relaxation delay = 20 s. The correction factors are listed in Table 2.3.

Table 2.3. Correction factors applied to data obtained from quantified  $^{31}\text{P}$  NMR signals to calibrate for incomplete relaxation of nuclei under experimental conditions.

$^{31}\text{P}$ nucleus	% unrelaxed/fully relaxed	Correction factor
$\alpha$ -ADP	86.21	1.16
$\beta$ -ADP	80.00	1.25
$\alpha$ -ATP	60.98	1.64
$\beta$ -ATP	58.48	1.71
$\gamma$ -ATP	78.13	1.28

The standards were used as a basis for all data acquisitions and the calibrations were applied to all data acquired. As described in Chapter 3, consumption of glucose (and concomitant production of lactate) was monitored in suspensions of *L. lactis ssp cremoris* MG1363 control cells, MG1363 titrated with acid in order to uncouple ATP consumption from biomass production, as well as mutants of MG1363 with over expressed *las* operon and overexpressed  $F_1$ -ATPase complex, respectively.

Cells in exponential growth phase (as determined in Section 2.1) were treated with glucose and  $[\text{U-}^{13}\text{C}]$ -glucose consumption (as identified by spectra of glucose standards, Section 2.3) was monitored, from which glycolytic fluxes were calculated per gram dry weight (Section 2.2). For each condition influencing the glycolytic flux, ATP/ADP ratios were determined (ATP and ADP identified as described in Section 2.4) and all glucose, lactate, ATP and ADP peak areas from rapidly pulsed spectra were calibrated for complete relaxation (Section 2.5).

## CHAPTER 3: PERTURBING ATP SUPPLY AND DEMAND IN NON-GROWING FERMENTING *L. LACTIS*

### 3.1 Introduction to experimental results

With the aim of quantifying changes in the steady state flux and ATP/ADP ratio in response to perturbations in glycolysis (supply) or ATP consumption (demand), the rate of  $^{13}\text{C}$ -glucose degradation and associated  $^{31}\text{P}$ -ATP/ADP ratio were measured in wild type *L. lactis* ssp *cremoris* MG1363 cells, untreated or treated with uncoupler, as well as in mutant strains with genetic modifications in either the supply or demand pathways. Supply-demand analysis was then performed to determine the locus of control over the steady state flux and ATP/ADP ratio.

Data presented in this chapter were acquired from two experimental batches in which cell suspensions of OD 80 (221 mg dry weight /ml) were used. Each batch was done in duplicate for all conditions. Each sample cell suspension was made up in 10 %  $\text{D}_2\text{O}$  and with a final 33 mM MES concentration.

Both batch experiments involved fermentations monitored *in vivo* by  $^{13}\text{C}$  NMR on a 600 MHz spectrometer, followed by fermentations performed on the bench, which were quenched at selected time points and extracts from these cells were analysed for  $^{31}\text{P}$  on a 400 MHz spectrometer. Each batch consisted of the reference strain MG1363, which was titrated step-wise with increasing concentrations of sodium acetate, as well as the mutant strains BK1506 (overexpressed ATPase  $\text{F}_1$ -complex) and CS8 (overexpressed *las* operon), both of which are described in Chapter 5.

Two minutes after adding glucose, the fermentations monitored *in vivo* by  $^{13}\text{C}$  NMR were rapidly pulsed (pulse length of 3.1  $\mu\text{s}$ , applied approximately every 1.7 s) as described in Chapter 5. The cumulative FIDs for every 2 minute interval underwent Fourier transformation, yielding spectra on which resonance frequencies for different nuclei can be distinguished (Figure 3.1).

While the experimental conditions yielded satisfactory *in vivo* signal intensity for  $^{13}\text{C}$  spectra, the signal intensity was too low to detect  $^{31}\text{P}$ . Attempts at optimising conditions (e.g. increasing the cell density and accumulating a greater number of FIDs per spectrum) to detect  $^{31}\text{P}$  *in vivo* were unsuccessful. The preparation and analysis of cell extracts was chosen as an alternative approach, during which  $^{31}\text{P}$  metabolites could be concentrated in cell-free solution and analysed at length using optimal NMR parameters.

Since MG1363 has shown a poor tolerance for the decrease in pH resulting from its own lactate production [19], a high buffer concentration was required (33 mM MES). Cell suspensions had to be given sufficient glucose for the  $^{13}\text{C}$ -glucose to be detectable, but not so much that they would produce too much acid or take too long to fully metabolise the glucose. Time constraints also made it necessary to use only as much glucose as could be completely consumed within 30 min. After some optimization, using cell suspensions at OD 60-80 and adding 40 mM glucose proved to result in the best metabolic viability for the cells. However, 40 mM unlabelled glucose still yielded a low signal on Fourier transformed spectra and in order to improve the signal, 40 mM glucose was used in the form of a 1:3 mixture of [ $^{13}\text{C}$ ] glucose: unlabelled glucose. This mixture would have a theoretical concentration of 10.33 mM  $^{13}\text{C}$ -glucose (or 25.825 %, based on a 1.1 % natural abundance of  $^{13}\text{C}$ ).

### 3.2 $^{13}\text{C}$ NMR for flux determination

Both glucose degradation and lactate production were monitored as indicators of the glycolytic flux. All twelve  $^{13}\text{C}$ -glucose peaks and all three  $^{13}\text{C}$ -lactate peaks were detectable in the +20 to +200 ppm range. MES was used as internal reference, as described in Chapter 5. All raw NMR data were processed using MestreNova 6.2.0 [75]. Spectra were subjected to phasing and baseline correction using the software tools. Peaks were selected based on standards (Figure 2.3) and were integrated manually using the processing software's manual integration tool.

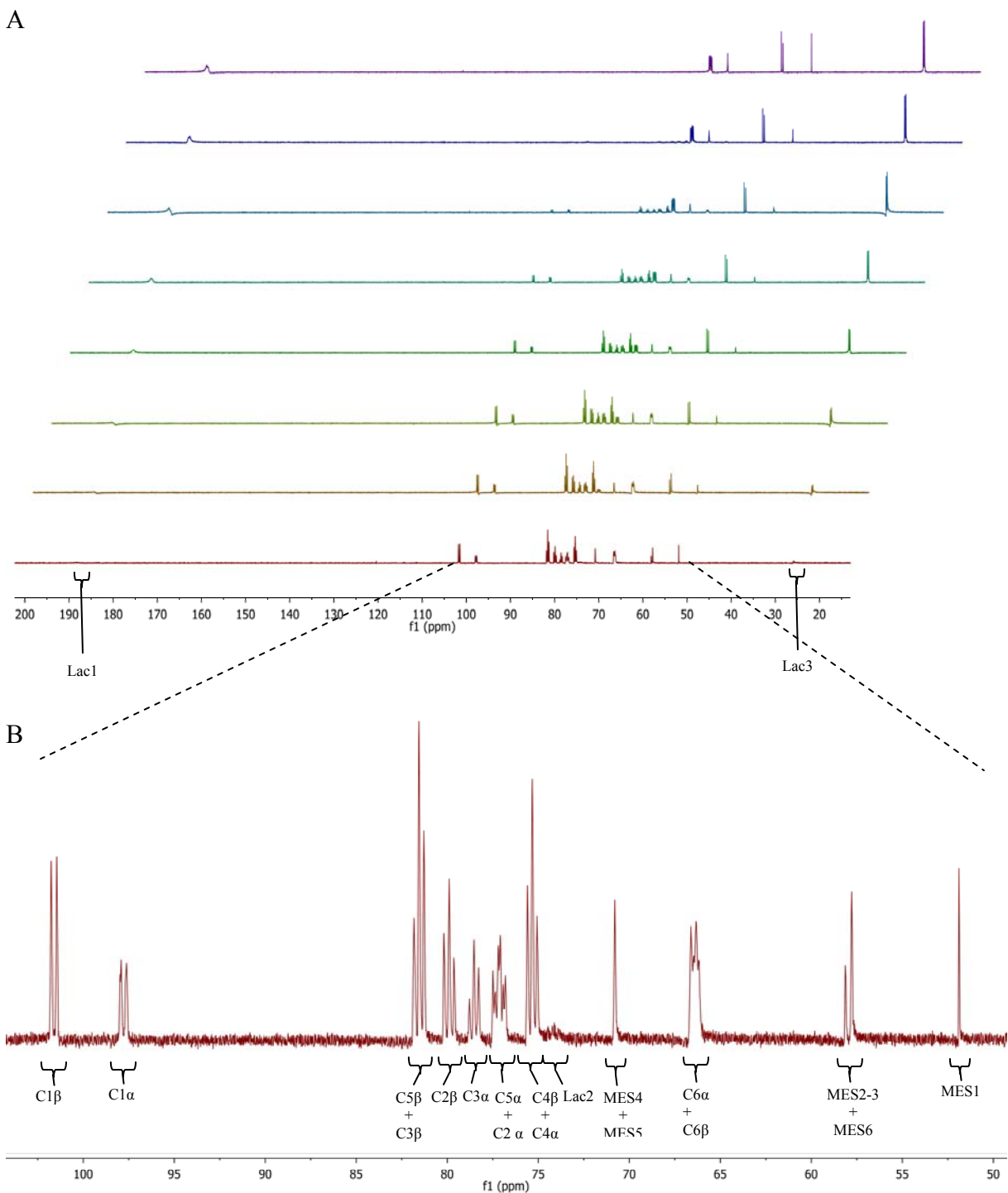


Figure 3.1. Time course  $^{13}\text{C}$  spectra representing 3, 5, 7, 9, 11, 13, 15, 17 and 19 min of fermentation, starting 2 min from addition of 30 mM glucose + 10 mM  $[\text{U-}^{13}\text{C}]$ -glucose. Samples were analysed *in vivo* on a Varian Unity 600 MHz spectrometer (see Chapter 5 for NMR parameters). Peak annotations are as determined by means



of glucose standards (Figure 2.3). A (spectrum range -200 to +20 ppm): lactate carbons 1 and 3 (Lac1 and Lac3); B (expansion of A range +105 to -50 ppm): glucose carbons 1-6 for both the  $\alpha$  and  $\beta$  anomers (C1-6 $\alpha$  and C1-6 $\beta$ ), lactate carbon 2 (Lac2) and carbons 1-6 of the internal standard, MES, (MES1-6).

Theoretically all the peaks representing nuclei belonging to the same molecule should have the same integratable area beneath them. However, it is clear from the spectrum in Figure 3.1 that this is not the case. As discussed in Chapter 2, some nuclei take longer than others to resonate and relax back to their original state. Since in all experiment samples were rapidly pulsed and the relaxation delay of 1 s may not be sufficient for all nuclei to return to a fully relaxed state, the resonance signal may not be fully detected for some peaks (eg. the three lactate peaks, which differed markedly in their signal intensity). Glucose and lactate readings were therefore calibrated for different relaxation times by means of a  $T_1$  experiment (as described in Chapter 2) to estimate their fully relaxed signal intensities.

Split peaks, as seen on the spectrum in Figure 3.1, result from minute electromagnetic interactions between a nucleus and its neighbouring nuclei (Section 1.5.1.4). Carbon-13 nuclei with two adjacent nuclei will result in two additional semi-distinguishable peaks, as the nucleus will interact slightly with each of them and will demonstrate slightly deviating chemical shifts. Such a multiplet of peaks must be integrated together, since it does not represent different nuclei, but the same nuclei resonating at two or three minutely different resonance frequencies.

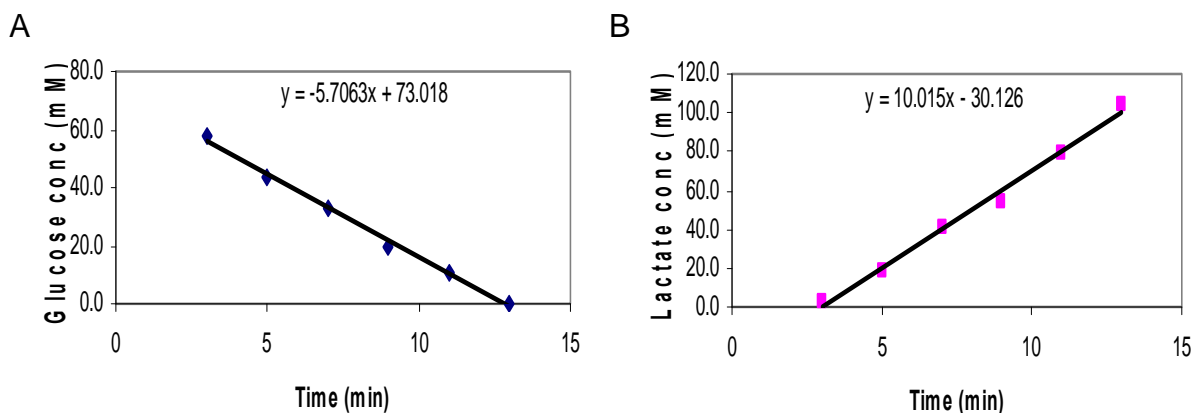


Figure 3.2. Glucose consumption (A) and lactate production (B). Data obtained from manual integration of peaks in MestreNova 6.2.0 software were normalised to values obtained for MES peaks, as standard for each spectrum. Linear regression was performed to determine the glucose and lactate fluxes.

The areas under all the glucose peaks were added together and the total normalised to the internal standard, MES, in order to compensate for variations in sensitivity. This yielded a dimensionless value which was determined for each time point in order to monitor the consumption of glucose concentration (Figure 3.2A). The same was done to monitor lactate production (Figure 3.2B).

Table 3.1. Glucose and lactate fluxes (flux  $\pm$  standard error,  $n = 4$ ) and the stoichiometric ratio between the rates of lactate production and glucose consumption. Fluxes are shown as signal intensity of  $^{13}\text{C}$ -glucose and  $^{13}\text{C}$ -lactate, normalised to MES (which remains constant throughout the fermentation experiment). These values were obtained from two batch cultures (each batch done in duplicate). The values in brackets next to the MG1363 strain indicate the concentration of added acetate.

	Glucose flux ( $\text{min}^{-1}$ )	Lactate flux ( $\text{min}^{-1}$ )	$V_{\text{lac}}/V_{\text{glc}}$
MG1363	$6.9 \pm 1.6$	$8.4 \pm 0.8$	$1.22 \pm 0.31$
MG1363 (+2mM)	$11.9 \pm 1.8$	$18.7 \pm 2.7$	$1.57 \pm 0.33$
MG1363 (+4mM)	$14.3 \pm 2.6$	$19.0 \pm 3.0$	$1.33 \pm 0.32$
BK1506	$11.9 \pm 2.6$	$11.2 \pm 1.9$	$0.94 \pm 0.26$
CS8	$5.6 \pm 0.7$	$6.5 \pm 1.7$	$1.16 \pm 0.34$

As shown in Table 3.1, stoichiometry of lactate produced per glucose consumed varied. The stoichiometries of  $v_{\text{lac}}/v_{\text{glc}}$  were below the 2.00 expected from homolactic fermentation and were within the range of 1.1-1.6 for all strains and conditions.

An unexpected result is the reduction in glucose and lactate flux in the *las*-overexpression mutant: the increased expression of PFK would be expected to keep triose phosphate levels high enough to keep GAPDH active to a high capacity, and overexpression of PK and LDH would be expected to maintain an elevated flux to lactate. Potential explanations for this are further explored in Chapter 4.

Reference strain MG1363 was titrated with 2 and 4 mM sodium acetate in order to observe and quantify the effect of an uncoupler in the flux. An effect was indeed observed with respect to the control (MG1363 with no sodium acetate), as shown in Figure 3.3.

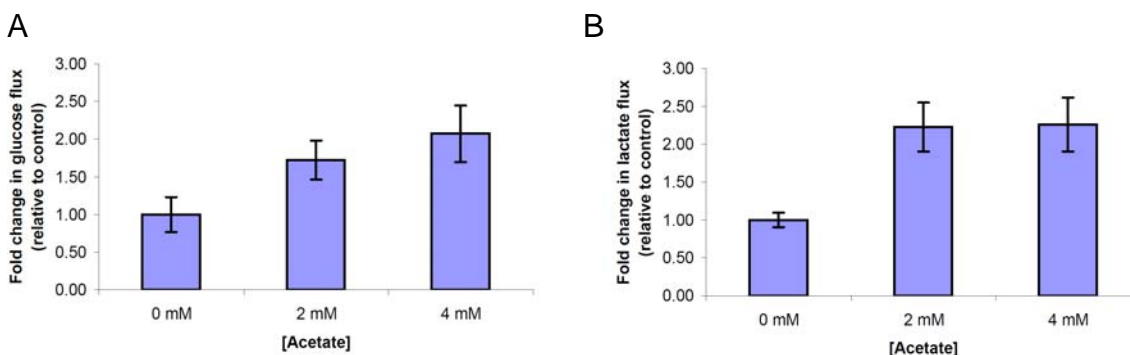


Figure 3.3. Fold change (A) glucose and (B) lactate fluxes in response to incubation with uncoupler (pre-incubation ~10 min prior to starting fermentation), at increasing concentrations ( $n = 3-7$ , standard error shown). Changes are shown as fold change compared to control (untreated wild-type).

The glucose flux increased with increasing concentrations of uncoupler, with 4 mM showing the greatest increase. Lactate flux also increased steadily in response to titration with uncoupler (although the lactate flux does not increase further in response to treatment with 4 mM uncoupler in comparison with 2 mM uncoupler, it nevertheless remained elevated over untreated control flux). In order to investigate whether a further

increase in lactate flux could be achieved, cells were treated with an even higher sodium acetate concentration. Treatment with 8 mM sodium acetate was found to be detrimental to cell survival and caused glycolysis to come to a near halt (data not shown). This is speculated to be due to the detrimental effect of acidification on MG1363, or perhaps an increased salt concentration due to buffering of the acid. Another possibility is that the  $H^+$ -ATPase could pump out the dissociated  $H^+$  quickly enough, causing cytoplasmic accumulation of  $H^+$ , weakening the cross-membrane proton-motive force (PMF).

### 3.3 $^{31}P$ NMR for ATP/ADP determination

The energy state of the cell was characterised by means of the ATP/ADP ratio. *In vitro* fermentations were halted by addition of perchloric acid and cells were lysed by freeze-thawing. Cell extracts were centrifuged to remove salt and proteins (as described in Chapter 5), neutralised, freeze-dried and resuspended in 15 %  $D_2O$ , and were analysed on a 400 MHz spectrometer in the -60 to +60 ppm range.

In Figure 3.4 the three multiplet ATP peaks and two multiplet ADP peaks are shown in the -22 ppm to +2 ppm range, as well as the internal reference, TEP, as identified previously by means of standards (Figures 2.4-2.6). As was observed for  $^{13}C$  spectra, the relaxation delay may not be sufficient for all nuclei to become fully relaxed after each pulse and a  $T_1$  experiment was performed (as described in Chapter 2) to calibrate each peak to fully relaxed signal intensity.

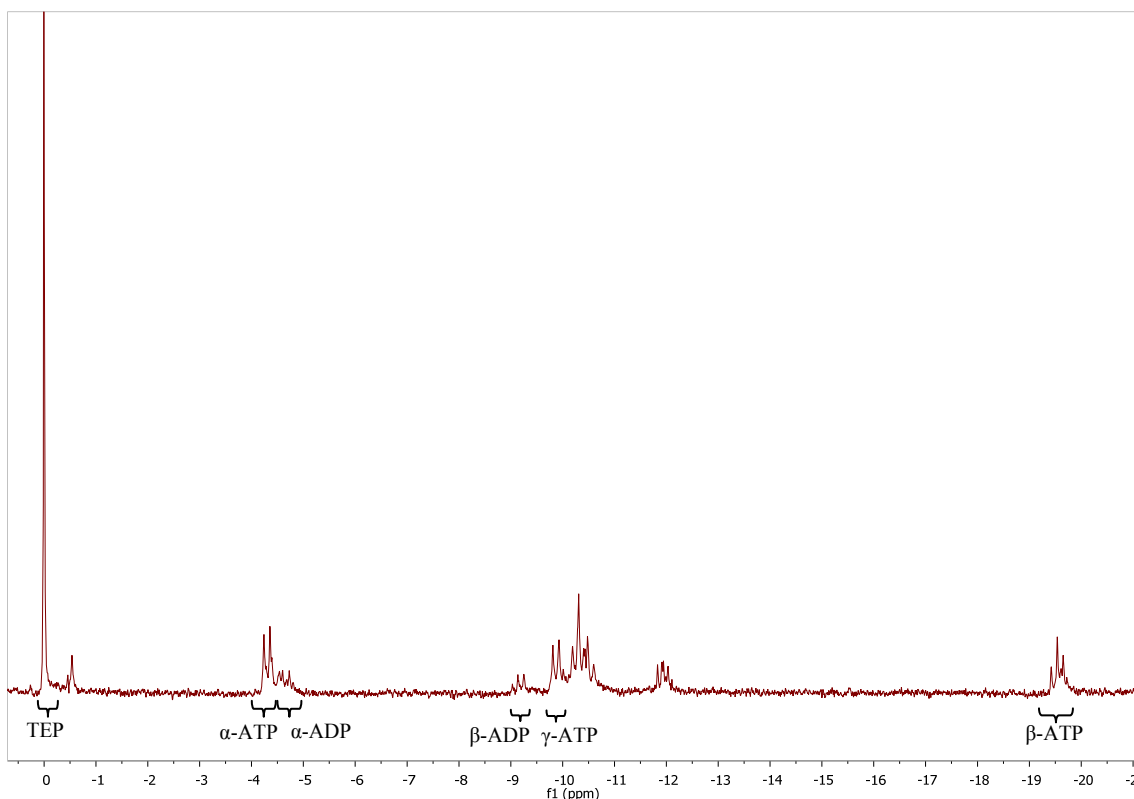


Figure 3.4. Fourier transformed  $^{31}\text{P}$  spectrum. Fermentations at an OD identical to those of the  $^{13}\text{C}$  fermentations were halted at various time points, extracts were prepared and dissolved in 15 %  $\text{D}_2\text{O}$ . These were analysed on a Varian Unity 400 MHz spectrometer (see Chapter 5 for NMR parameters).

As in  $^{13}\text{C}$  spectra, the phenomenon of peak splitting can be clearly observed in Figure 3.4 and split peaks were again treated as components of a single nucleus signal. The ATP/ADP ratios for the wild-type (with and without sodium acetate), the *las* mutant and the  $\text{F}_1$ -ATPase mutant are shown with standard errors in Figure 3.5. A miniscule increase in ATP/ADP was observed in the *las*-overexpression mutant (CS8), however a greater increase in ATP/ADP was seen in the  $\text{F}_1$ -ATPase mutant. The latter was rather unexpected, since overexpression of the  $\text{F}_1$ -ATPase was expected to have the same effect on ATP/ADP as incubation with an uncoupler, i.e. a lower ATP/ADP than the wild type.

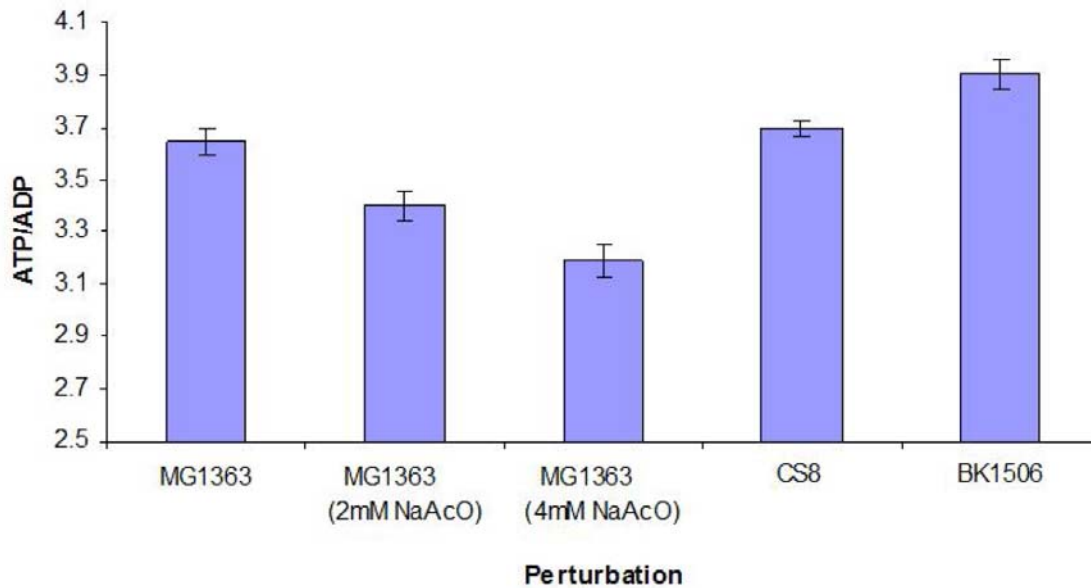


Figure 3.5. ATP/ADP ratios determined in cell-free extracts ( $n = 3$ ) for wild-type strain MG1363 titrated with sodium acetate, as well as for mutant strains BK1506 and CS8 (described in Chapter 2). Standard errors are shown. Wild-type MG1363 without uncoupler was used as control in all cases. Raw data were normalized to the internal standard, TEP, and calibrated for relaxation status by means of a  $T_1$  experiment (described in Chapter 2).

### 3.4 Supply-demand analysis

In order to investigate the effect of certain perturbations on the glycolytic flux and the resulting energy state on the cell (described by means of the ATP/ADP ratio), percent change in the glycolytic flux with respect to the wild-type untreated control was plotted against the ATP/ADP ratio (Figure 3.6).

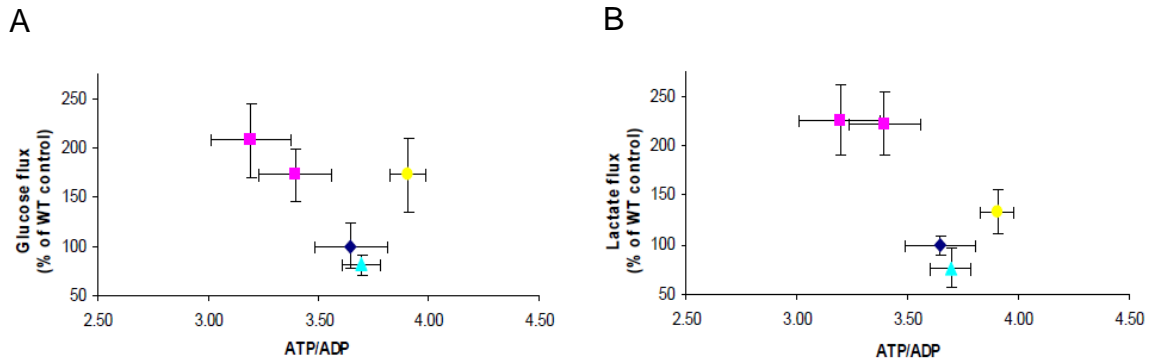


Figure 3.6. Variation of (A) glucose and (B) lactate fluxes with ATP/ADP ratios ( $n = 3-7$ ), with standard error. All fluxes are shown in relation to the wild-type untreated control ( $\blacklozenge$ ). The supply perturbation is shown by ( $\blacktriangle$ ). The demand perturbations with uncoupler and overexpressed  $F_1$ -ATPase produced data points ( $\blacksquare$ ) and ( $\bullet$ ), respectively.

Addition of 2 mM and 4 mM sodium acetate resulted in an increase in both glucose and lactate fluxes and a decrease in ATP/ADP (Figures 3.5-3.6). While the mutant BK1506 (with overexpressed  $F_1$ -ATPase) also resulted in higher glucose and lactate fluxes with respect to the wild type, ATP/ADP was found to be slightly higher than in the wild-type. The mutant CS8 demonstrated slightly reduced glucose and lactate fluxes, while ATP/ADP was higher respect to the wild-type.

The data from Figure 3.6 were converted to a double-log scale and each perturbation plotted separately with untreated wild type (WT), as shown in Figure 3.7 (A-F). On a logarithmic scale, the elasticity ( $\epsilon$ ) of the supply pathway (glucose and lactate fluxes) to changes in ATP/ADP can be calculated.

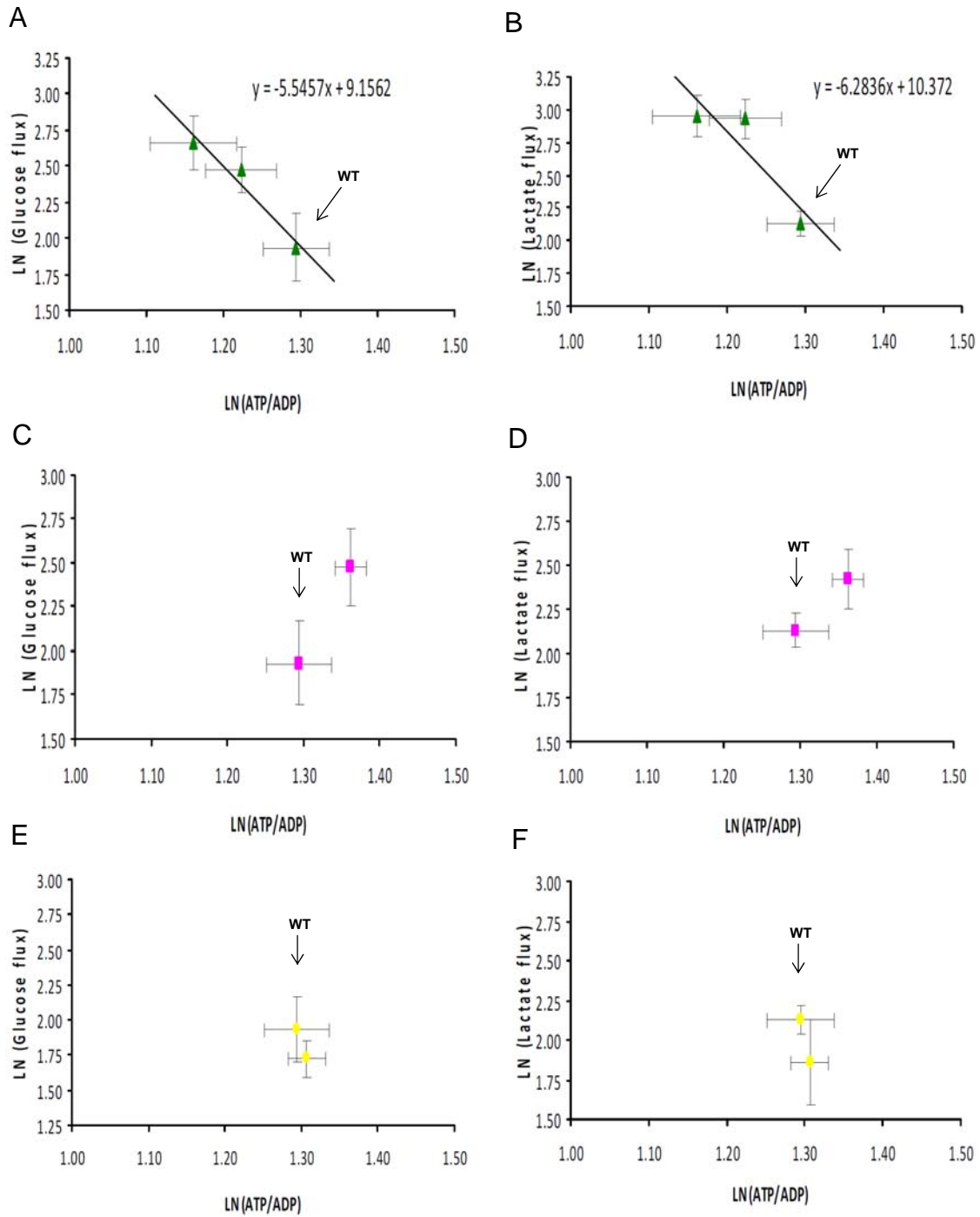


Figure 3.7. Rate characteristics of demand perturbation by means of uncoupler titration (A and B), overexpressing ATPase F<sub>1</sub> subunits (C and D) and supply perturbation by over-expression of the *las* operon (E and F).



The elasticities of the glucose and lactate fluxes to changes in ATP/ADP were found to be -5.6 and -6.3, respectively (Figure 3.7, A and B). No elasticities could be calculated in the case  $F_1$ -ATPase overexpression (Figure 3.7, C and D) and *las* operon overexpression (Figure 3.7, E and F), as a single perturbation is not sufficient for determination of rate characteristics.

The data presented in this chapter will be further interpreted and discussed in Chapter 4. Since the experimental data acquisition is intended to culminate in the calculation of elasticities, the extent to which this has been achieved is put in perspective of the determination of complete rate characteristics for energy supply and demand. The methodology by which the data were acquired is described in more detail in Chapter 5.

## CHAPTER 4: DISCUSSION

### 4.1 Synopsis

Treatment of exponential growth-phase cells with 2 mM sodium acetate resulted in a 72 % increase in rate of glucose consumption and a 123 % increase in lactate production, as determined *in vivo* by  $^{13}\text{C}$  NMR. Treatment with 4 mM sodium acetate led to a 107 % increase in glucose consumption and a 126 % increase in lactate production, with respect to untreated cells. This was accompanied by a ~6.9 % and ~12.4 % decrease in ATP/ADP in response to 2 mM and 4 mM acetate, respectively.

In mutant strain BK1506, with overexpressed  $\text{F}_1\text{-ATPase}$ , rates of glucose consumption and lactate production respectively were 72 % and 33 % higher than in the wild type MG1363. ATP/ADP was 1.3 % higher with respect to wild type. Mutant strain CS8, with overexpressed *las* operon, demonstrated a 19 % and 24 % reduction in glucose and lactate flux with respect to the wild type MG1363, as well as 7 % increase in ATP/ADP.

The response of the ATP supply pathway to changes in ATP (by increasing ATP demand) was quantified by determining the elasticity of the supply to changes in ATP/ADP. However, treatment of MG1363 cells with acid proved to have detrimental effects on glucose metabolism and cell viability, making it a non-ideal method of perturbing ATP demand. Manipulating expression of enzymes key to either ATP supply or ATP consumption was investigated as an alternative and more selective approach.

The methods applied in this study, their pros and cons, and the results obtained will be further analysed and discussed in context in the next section.

### 4.2 Discussion

#### 4.2.1 NMR as analytical technique

In this study, the benefit of NMR as a non-invasive, real-time (online) method to measure metabolite concentrations was exploited in order to monitor carbon flux ( $^{13}\text{C}$ -NMR).

However, attempts to perform the same analysis by  $^{31}\text{P}$ -NMR were not successful as little or no  $^{31}\text{P}$  was detectable in the samples. In order to investigate whether this was due to low cell mass (and thus undetectable cytoplasmic  $^{31}\text{P}$  metabolites), cell suspensions of OD as high as 300 were used, to no avail. This led to the utilisation of extraction techniques in order to isolate and concentrate adenine nucleotides from lysed cells.

NMR is a notoriously insensitive technique, particularly for detection of  $^{13}\text{C}$ . The precision of phasing and baseline correction can affect the calculated peak areas, which can lead to an even greater error margin when data is dependent on ratios between peaks. Very small changes detected in glucose or lactate concentrations may thus not be accurate enough to serve as a basis for deductions regarding differences between wild-type/untreated and mutant/treated cells.

The non-homogeneity of the can also contribute to the relative inaccuracy of the technique. A sample volume of 3 ml was required for analysis and the cell mass in this volume needed to be optimised for rate of glucose consumption (good resolution of data points), as well as experimental duration (a logistical constraint when using batch cultures). However, higher ODs tend to result in settling out of the cells, resulting in a higher OD at the bottom of the sample tube than at the top. As the experiment progresses, the OD of the cell suspension might therefore change at the specific point in the sample tube where the signal is detected by the RF-coils of the spectrometer.

Deductions made from experimentally-acquired data, as will be discussed further in this chapter, must thus be made with these factors in mind.

#### *4.2.2 Wild-type fermentation patterns*

The stoichiometric ratio of lactate produced per molecule of glucose consumed was not the expected two lactate molecules to one molecule glucose. Possible causes for this deviation from the expected stoichiometry include: A) Non-homolactic fermentation - pyruvate was not exclusively being converted to lactate by LDH but was entering alternative metabolic branches. However, the end-products of other pyruvate branches

(mixed acid fermentation) have  $^{13}\text{C}$  nuclei that fall within the 0-200 ppm chemical shift scale in relation to MES  $^{13}\text{C}$  nuclei (Table 4.1) [66, 67]. None of these end-products were detected within the chemical shift range scanned, indicating there was no accumulation of any fermentation products other than lactate.

Table 4.1. Chemical shifts of alternative products of pyruvate metabolism

Product of pyruvate metabolism	$^{13}\text{C}$ NMR chemical shift (ppm)
Ethanol	18.1, 57.8
Acetone	29.9, 206.7
2,3-butandione (di-acetyl)	20.0-40.0

B) Cell suspension was not homogenous - settling of cells in the sample tube during the experimental period (Section 4.2.1) may have resulted in an increasing signal for both glucose and lactate lower in the sample tube, while the signal intensity decreased higher up in the tube. While glucose was observed to decrease over time, this non-homogeneity may have resulted in an inaccurate estimation of the lactate to glucose ratio.

#### 4.2.3 Lactate production

As discussed in Chapter 1, production of lactate results in a lowered pH in the cytoplasm and extracellular environment [20]. In this study, a pH change from ~6.5 to ~5.0 was observed after fermentation of 40 mM glucose under non-growing conditions, despite high extracellular buffer concentration (data not shown). It was observed that cells in culture entered stationary growth phase at an unexpectedly low OD. This may have resulted from the choice of growth medium, which is recommended for lactic acid bacteria, but perhaps not ideal for the particular requirements of *Lactococcus lactis*. Also, glycolysis may be slightly slowed in response to the decrease in pH resulting from the degradation of glucose in the growth medium [67]. A decreased cellular pH dissipates the cross-membrane proton motive force (PMF), activating the  $\text{H}^+$ -translocating  $\text{F}_1\text{F}_0$ -ATPase, which consumes increased amounts of ATP in order to maintain the intracellular pH (and PMF) in an acidic extracellular environment [68, 69]. The result is a decrease in availability of ATP for biomass production and perhaps an inability of glycolysis to keep

up with the cell's ATP requirements. However, as would be expected from a high glycolytic rate, fermentation was found to be homolactic in these cells even at reduced pH, as was deduced by the fact that even at pH 5.0 (post-fermentation) only lactate was produced.

#### 4.2.4 Demand perturbations

##### 4.2.4.1 Treatment of wild-type *L. lactis* with uncoupler

Wild-type *L. lactis* was treated with weak acids in order to dissipate the transmembrane PMF and activate the H<sup>+</sup>-translocating ATPases. When wild-type *L. lactis* ssp *cremoris* MG1363 was treated with 0-8 mM sodium benzoate (10 min prior to glucose addition), little to no change was observed in terms of both the glycolytic flux and ATP/ADP ratio (data not shown). However, treatment with 2 mM sodium acetate (10 min prior to glucose addition) resulted in a 72 % increase in glucose flux and 123 % increase in lactate flux. Treating with 4 mM sodium acetate yielded an increase of 107 % in glucose flux and 126 % increase in lactate flux.

The difference in effect between sodium benzoate and sodium acetate could be due to the difference in strengths of the two acids – benzoic acid has a pKa of ~4.2 and is a stronger acid than sodium acetate (pKa ~4.7). At the experimental pH range of 5.5-6.5, sodium benzoate is more dissociated than sodium acetate. Considering the sensitivity of *L. lactis* to acidity, benzoate may have been overloading the proton-pumping ATPases. A weaker acid such as acetate may achieve the desired effect of increasing the activity of the proton pumps without overloading the cell's capacity to cope with acid stress.

Attempts were made to minimise the effect of lactate production in the extra-cellular pH during fermentation by resuspending the cells in a high buffer concentration (500 mM MES stock). This could also have the potential effect of buffering the dissociated acetic acid, thereby reducing the uncoupling effect of adding an acid.

Nevertheless, the observed increase in glycolytic flux (both in glucose consumption and in lactate production) was accompanied by a 1.07 fold decrease in ATP/ADP (at 2 mM

sodium acetate) and a 1.14 fold decrease in ATP/ADP (at 4 mM sodium acetate). Despite some overlap of ATP/ADP error bars (Figure 3.5), these data indicate that even at a high buffer concentration, sodium acetate appears to result in increased consumption of ATP by H<sup>+</sup>-ATPases.

#### 4.2.4.2 Elasticity coefficients

A living cell has to maintain a metabolic steady state, at which the rate of supply of a central metabolite (in this case, the free-energy metabolite ATP) is equal to the rate of consumption of that metabolite. Perturbations to either the supply or demand blocks can force the metabolic system into a transient state where it attempts to achieve a new steady state, at which the rate of consumption of the central metabolite again equals its regeneration [48].

Ideally, supply-demand analysis would involve a double-modulation approach, i.e. the supply and demand pathways would be modulated in turn and the resultant steady-state supply and demand fluxes and steady-state ATP/ADP values determined. However, since there are various different reaction pathways making up the ATP-demand block, the demand flux would be extremely difficult to determine. We therefore make the assumption that, during steady state, the flux of the ATP supply block is more or less equal to the flux of the ATP demand block.

ATP and ADP were sampled during linear rate of glucose consumption in order to confirm that the cells had attained a quasi-steady state. Each experimentally-acquired point therefore represents a new steady state attained under different levels of perturbation with uncoupler. The sensitivity of the supply pathway to changes in ATP/ADP (in response to perturbations in the ATP demand pathway) was determined by plotting the flux and ATP/ADP on a double natural logarithmic scale. The elasticity coefficients can be determined by calculating the slope of this rate characteristic curve at the steady state point.

Section 1.4.1 summarised some equations defining the control one of the reaction blocks has on the steady state flux or metabolite concentration in terms of control coefficients, and in Section 1.4.2 the elasticities of the supply and demand pathways with regard to ATP/ADP are defined. In a complete control analysis study, the elasticity coefficients can be used to calculate the control coefficients for the flux in response to changes in local rates of the supply and demand pathways. However, the supply elasticities determined in this study are very high compared with the same determined for yeast (-0.84 [41]) and *E. coli* (-0.07 [71]), and even without having both supply and demand elasticity values certain deductions can be made about the concentration control coefficients ( $C_{\text{supply}}$  and  $C_{\text{demand}}$ ) from the magnitude of the available elasticity:

**Connectivity theorems** [70] state that flux control coefficients and elasticities around a single pathway intermediate (in the context of supply-demand) relate to one-another as follows:

$$C_{\text{supply}}^J \cdot \varepsilon_{\text{ATP/ADP}}^{\text{supply}} + C_{\text{demand}}^J \cdot \varepsilon_{\text{ATP/ADP}}^{\text{demand}} = 0 \quad [\text{Eq. 28}]$$

Therefore:

$$C_{\text{supply}}^J \cdot \varepsilon_{\text{ATP/ADP}}^{\text{supply}} = -C_{\text{demand}}^J \cdot \varepsilon_{\text{ATP/ADP}}^{\text{demand}} \quad [\text{Eq. 29}]$$

From this relationship, we can deduce the relative magnitudes of the flux control coefficients and elasticity coefficients of the two pathways:

$$C_{\text{supply}}^J / C_{\text{demand}}^J = - \varepsilon_{\text{ATP/ADP}}^{\text{demand}} / \varepsilon_{\text{ATP/ADP}}^{\text{supply}} \quad [\text{Eq. 30}]$$

From this connectivity theorem, it is clear that if the demand elasticity ( $\varepsilon_{\text{ATP/ADP}}^{\text{demand}}$ ) has a high absolute value relative to the supply elasticity ( $\varepsilon_{\text{ATP/ADP}}^{\text{supply}}$ ), that the flux control coefficient of the supply pathway ( $C_{\text{supply}}^J$ ) would have a high absolute value with relation to the flux control coefficient of the demand pathway ( $C_{\text{demand}}^J$ ). If, however, the absolute value of the elasticity of the supply pathway ( $\varepsilon_{\text{ATP/ADP}}^{\text{supply}}$ ) is greater, the opposite is true.

A high supply elasticity suggests that a greater amount of flux control may lie in the demand pathway, i.e. that  $C_{\text{demand}}^J > C_{\text{supply}}^J$  (although this cannot be stated with certainty, as the demand elasticity was not determined).

A further deduction can be made from the magnitude of the supply elasticity, concerning the concentration control coefficient, which is related to the elasticities of the supply and demand pathways as follows:

$$C_{\text{supply}}^{\text{ATP/ADP}} = 1 / (\epsilon_{\text{ATP/ADP}}^{\text{demand}} - \epsilon_{\text{ATP/ADP}}^{\text{supply}}) \quad [\text{Eq. 31}]$$

$$C_{\text{demand}}^{\text{ATP/ADP}} = -1 / (\epsilon_{\text{ATP/ADP}}^{\text{demand}} - \epsilon_{\text{ATP/ADP}}^{\text{supply}}) \quad [\text{Eq. 32}]$$

If the absolute value of the supply elasticity is high, the absolute value of both  $C_{\text{supply}}^{\text{ATP/ADP}}$  and  $C_{\text{demand}}^{\text{ATP/ADP}}$  will be small. A high concentration control coefficient for either the supply or demand pathway permits greater potential fluctuation in ATP/ADP, suggesting the homeostasis of ATP/ADP is not very good. A high supply elasticity therefore indicates good ATP/ADP homeostasis, since ATP/ADP levels would not respond greatly to changes in either pathway and would be more stable.

Although the supply elasticities (for glucose and lactate flux) determined in this study are much greater than those determined in similar studies in other microbial organisms [41, 71], they are not completely outside the conceivable range of elasticities for reaction blocks. ATP/ADP would be “felt” at different levels by the supply block (HK, PFK, PGK and PK) and this combined effect may result in a large supply elasticity [72].



#### 4.2.4.3 F<sub>1</sub>-ATPase overexpression

Adding acid in order to increase ATP consumption by H<sup>+</sup>-pumping ATPases is an easy, *ad hoc* method by which to perturb ATP demand. However, metabolism of glucose by non-growing suspensions of MG1363 results in decreased pH – this accumulation lactic acid causes reduced biomass growth and glycolytic flux [73-75]. While adding uncoupler does appear to result in a decrease in ATP levels and a reactive increase in glycolytic flux, the flux is also influenced by the decrease in pH caused by lactate production. Therefore, the magnitude of the flux as determined by <sup>13</sup>C NMR spectroscopy may not be a true reflection of the flux response to changes in ATP/ADP. This begs for an alternative approach to perturbing the rate of ATP consumption other than reducing the extracellular pH.

An approach which meets these criteria would be to increase the concentration of ATP-hydrolyzing enzymes – i.e. rather than simply stimulating the activity of H<sup>+</sup>-translocating ATPases, one could generate strains with higher concentrations of these enzymes, thereby reducing the effect of pH on the system. Koebmann *et al.* [46] overexpressed the F<sub>1</sub>-subunit of the F<sub>1</sub>F<sub>0</sub>-ATPases in order to study the effect on ATP consumption in steadily-growing cells. Since our study does not look into the control of individual enzymes on the overall steady state flux, but considers ATP producing and consuming processes as composite reaction blocks, the F<sub>1</sub>F<sub>0</sub>-ATPase is seen as contributing to the entire ATP-consuming (demand) block rather than being studied for its individual control over the flux. Modulating expression of the *atp* operon (or a part thereof) of this enzyme provides a means by which to perturb the ATP demand block in order to study the effect on  $v^{\text{supply}}$ . A mutant with overexpressed  $\alpha$ ,  $\beta$  and  $\gamma$  subunits of the F<sub>1</sub>-ATPase was grown alongside a wild-type reference strain MG1363. The two strains were comparatively analysed by means of *in vivo* NMR spectroscopy in terms of glucose and lactate fluxes and ATP/ADP (Chapter 5).

Increasing the expression of F<sub>1</sub>-subunits of the F<sub>1</sub>F<sub>0</sub>-ATPase was expected to have the same effect as increasing the activity of this ATPase by adding uncoupler. As expected, glucose and lactate fluxes were elevated in relation to wild-type MG1363 (Table 3.1).

However, unlike MG1363 treated with sodium acetate, ATP/ADP levels appeared to increase slightly (Figure 3.5). This is in contrast to what was observed by Koebmann *et al.* [46, 55]: ATP and ADP concentrations from cells extracts by indirect luciferase-based method showed a gradual decrease in ATP/ADP in response to increases in F<sub>1</sub>-ATPase activity.

One potential explanation for this discrepancy is the choice of growth medium. In the affore-mentioned study, BK1506 cells were grown in SA medium supplemented with glucose. In the study discussed here, all strains were grown in MRS broth (described in Chapter 5). MRS broth (recommended for lactic acid bacteria) is supplemented with sodium acetate to reduce the growth of competitive bacterial species. It is conceivable that this exposure to sodium acetate during growing conditions, combined with the increased concentration of F<sub>1</sub>-ATPase in the mutant BK1506, puts such strain on the ATP/ADP levels that the supply pathway responds by transcriptional upregulation of glycolytic enzymes in order to keep up with the ATP demand. If this upregulation is maintained during non-growing conditions (in medium-free buffer suspension), the rate of ATP generation by the supply pathway would remain elevated even though the ATP consumption may relax slightly in the absence of sodium acetate.

Another factor to consider is that MG1363 is not the recommend reference strain for BK1506. The recommended reference strain for this mutant is BK1010 (MG1363 transfected with a promoter probe vector). However, the control used in this study was the untransfected untreated control strain MG1363. Whether the transfected vector alone would have a negative effect on glycolysis (and thereby ATP production) is not known and would need to be taken into consideration in a quantitative expression study.

Judging from these results, it is speculated that a higher steady state ATP/ADP is maintained where the supply pathway has adapted to the combined demand of increased ATPase concentration combined with mild acid-stress during growing conditions.

#### 4.2.5 Supply perturbation

##### 4.2.5.1 *Las* operon overexpression

The *las* operon encodes the three glycolytic enzymes PFK, PK and LDH [76]. None of these enzymes has been definitively attributed a high flux control during homolactic fermentation, however their overexpression has been shown to inhibit alternate pyruvate branches and promote homolactic fermentation [45, 47]. A rapid glycolytic flux, as promoted by upregulation of PFK, ensures high levels of triose phosphates to inhibit PFL and high levels of FBP to activate LDH. However, in studies using various levels of over-/underexpression, both increase and reduced expression of the *las* operon have been shown to result in a slightly reduced glycolytic flux [28]. A 10 % decrease in *las* operon expression has been found to result in an increase in mixed acid fermentation [77] – further evidence that this operon promotes homolactic fermentation by inhibiting alternate enzymatic pathways from pyruvate.

The mutant CS8 was generated by Solem *et al.* [78] with an overexpressed *las* operon resulting in 200 % enzyme activity compared with the wild-type MG1363. Our results confirmed those of Solem *et al.* in that with two-times elevated *las* enzyme activity was found to result in a very small increase in ATP/ADP. However, contrary to expectation, a decrease was observed in both the glucose and lactate fluxes with respect to the wild-type MG1363 during fermentation on glucose].

The decrease in glycolytic flux in this mutant is rather perplexing – as previously mentioned, overexpression of PFK, PK and LDH would be expected to result in an increase in glycolytic flux. Instead, a 19 % and 23 % reduction was observed in the glucose and lactate fluxes, respectively. Furthermore, a reduced glycolytic flux would not be expected to be accompanied by an increase in ATP/ADP, rather the contrary would be expected.

The stoichiometric ratio between glucose consumed and lactate produced did drop slightly from 1.22 to 1.16 (Table 3.1). Although this is not a very significant decrease in stoichiometry, the low ratio does imply a deviation from homolactic fermentation. While

the insensitivity of NMR as a biological measurement of metabolite concentration might be partly to blame, it has also been considered that under anaerobic batch culture conditions, without continuous glucose supply, fermentation may not be entirely homolactic. Also, as with the mutant strain BK1506, the effect of transfection with a vector needs to be taken into consideration when referencing a mutant to an untransfected control strain.

Distribution of pyruvate between LDH and PFL may explain the incongruity of the minute increase in ATP/ADP despite the decrease in flux in the *las* mutant: pyruvate converted to formate and acetyl CoA, which is then converted to the end-product acetate, results in the production of an additional ATP per molecule pyruvate. This means that one might expect to see a slight increase in ATP/ADP ratio during mixed-acid fermentation. This speculation does, however, not explain why no glycolytic products other than lactate were detected by  $^{13}\text{C}$  NMR. Perhaps their concentrations were too low to be detected alongside the high concentrations of glucose and lactate present.

The reason for the reduction in glycolytic flux despite the overexpression of glycolytic enzymes also remains unexplained. It has been speculated [79] that the rapid flux of metabolites through glycolysis (eg. high PK activity) may be reducing the pools of allosteric activators and inhibitors, such as FBP and triose phosphates, which promote homolactic fermentation. Also, an increase in ATP consumption has been suggested to direct glycolysis to slower-fermenting pathways that produce more ATP per molecule glucose.

### **4.3 Future Work**

The complications arising from pH-sensitivity indicate that while the approach of demand perturbation by means of incubation with acid may be useful and practical for other bacterial strains (e.g. *E. coli*), it is less suitable for *L. lactis*, as the viability of the cells appears to be compromised at acid concentrations exceeding 4 mM.

Gene modulation, though more laborious, appears to be a better approach for perturbations of supply and demand pathways in *L. lactis*. Work by other groups [10, 46] has yielded mutants with modulations in both supply and demand pathway genes, providing ample opportunity to perform stepwise comparisons of steady state flux and ATP/ADP between different levels of overexpression of both F<sub>1</sub>-ATPase subunits and the *las* operon. However, the repetition of batch experiments with several mutant strains is laborious.

For complete supply-demand analysis, several levels of modulation of both the F<sub>1</sub>-ATPase and the *las* operon would be required in order to obtain rate characteristics for both the supply and demand pathways. This and previous studies have shown that these two enzymes are useful centres for modulation in the pursuit of potent gateways for perturbation of the supply and demand pathways.

#### **4.4 Conclusions**

While results in this thesis preclude a complete supply-demand analysis (due to insufficient data for the accurate determination of a demand elasticity), they do represent a basis for further experimental approaches to quantitative supply-demand analysis using the model *L. lactis* strain MG1363. Our results do suggest that a greater locus of control may lie in the demand pathway, as can be deduced from the relatively high supply elasticity.

## CHAPTER 5: MATERIALS AND METHODS

### 5.1. Culture methods (*Lactococcus lactis*)

#### 5.1.1 Bacterial strains

*Lactococcus lactis* strain MG1363, a plasmid-free derivative of NCOD0712, was used as reference strain. BK1506 (MG1363 transformed with pCPC7::*atpAGD* Erm<sup>r</sup> [46]) was used to study the effect of perturbing the ATP-demand pathway via F<sub>1</sub>-ATPase over-expression. CS8 (MG1363 transformed with random CP-*las*, obtained by single homologous recombination with pRC1-CP-pfk) shows a 2-fold over-expression of the *las* operon, which encodes phosphofructokinase (PFK), pyruvate kinase (PK) and lactate dehydrogenase (LDH), and was used to study the effects of perturbing the ATP-supply pathway [10, 28].

#### 5.1.2 Culture media

Cultures were grown in MRS broth (Merck) [80], with the following composition: 20.0 g/L glucose, 10.0 g/L special peptone, 5.0 g/L meat extract, 5.0 g/L yeast extract, 20.0 g/L dextrose, 2.0 g/L di-potassium hydrogen phosphate, 1.0 g/L Tween 80, 2.0 g/L tri-ammonium citrate, 0.1 g/L magnesium sulphate, 0.05 g/L manganese sulphate and 5.0 g/L sodium acetate. MRS agar has an identical composition, with 12.0 g/L agar added. Culture medium was prepared using deionised water and autoclaved at 121 °C for 15 min (as per manufacturer's recipe).

#### 5.1.3 Stocks

Stock cultures were frozen in 40 % (v/v) glycerol and stored in 2 ml aliquots at -80°C. New batch cultures were prepared by inoculation onto MRS agar plates.

#### 5.1.4 Bacterial cell culture

Agar-plate cultures were incubated for 24 hours at 30 °C. Pre-cultures (20 ml) were inoculated with a single colony and were incubated in a Gallenkamp Orbital Incubator at

30 °C and continuously shaken at  $\pm 150$  rpm. Experimental cultures (500 ml) were inoculated from these pre-cultures and incubated in the same manner.

#### *5.1.5 Cell harvesting*

Cells were harvested in late log phase: cultures were centrifuged for 5 min in a Beckman J2-21 centrifuge at 5000 rpm ( $3020\times g$ ) and 4 °C. The pelleted cells were washed twice with deionised water and resuspended in 500 mM MES buffer at pH 6.5.

#### *5.1.6 Reagents*

MRS broth, EDTA disodium salt, potassium carbonate, perchloric acid and deuterium oxide were acquired from Merck (Darmstadt, Germany). Glucose (cold), triethyl phosphate, adenosine triphosphate and adenosine diphosphate were acquired from Sigma-Aldrich (St Louis, USA). Labelled [U- $^{13}\text{C}_6$ ]-glucose was obtained from Cambridge Isotope Laboratories (Andover, USA). MES buffer was acquired from USB Chemical Laboratories.

## **5.2 $^{13}\text{C}$ NMR spectroscopy: Carbon fluxes**

### *5.2.1 In vivo fermentations*

Cell suspensions were prepared in 10 %  $\text{D}_2\text{O}$  and incubated at 30 °C. Fermentation was initiated by adding 40 mM glucose (of which: 10 mM [U- $^{13}\text{C}_6$ ]-glucose and 30 mM unlabelled glucose). Immediately after addition of glucose, concentrations of glucose and lactate were determined from  $^{13}\text{C}$  spectra at a resonance frequency of 150.8 MHz (600 MHz Varian Unity Inova NMR spectrometer, 10mm broad band probe). Starting 2 min after glucose addition (as  $t_0$ ), spectra were acquired and compiled into a time-scale array. Each  $^{13}\text{C}$  spectrum consisted of 71 FIDs, with the following parameters: pulse width = 6  $\mu\text{s}$ , acquisition time = 0.7 s, relaxation delay = 1 s, spectral width from -18 to 148 ppm. Spectra were acquired for approximately two minutes each and represented the cumulative scans taken over that time period.

### 5.2.2 Concentrations of $^{13}\text{C}$ metabolites from NMR data

Peaks representing glucose  $^{13}\text{C}_{1-6}$ , ( $\alpha$  &  $\beta$  anomers), as identified by means of the standards (Figure 2.3), were integrated using MestreNova 6.2.0 software's manual integration tool [81], which calculates the area under each peak. The area under each peak is proportional to the number of  $^{13}\text{C}$  nuclei represented by that peak, and the concentrations of the  $^{13}\text{C}$  nuclei can be calculated by comparing their peak areas to those of the internal standard, MES. Peak areas were calibrated for relaxation times, as described in Chapter 2 (Section 2.5).

## 5.3 $^{31}\text{P}$ NMR spectroscopy: ATP/ADP determination

Online measurements of  $^{31}\text{P}$  levels proved difficult and no  $^{31}\text{P}$  could be detected in vivo in cell suspensions identical to those used for  $^{13}\text{C}$  measurements. Even doubling the OD of cell suspensions yielded no detectable  $^{31}\text{P}$  resonance signal. In order to still be able to perform side-by-side measurements of  $^{31}\text{C}$  and  $^{31}\text{P}$  metabolites from the same batch cultures, metabolite extracts were prepared from the same batch which was used for in vivo NMR measurements.

### 5.3.1 Fermentations and cell extracts

Cell suspensions (OD 80, dry weight = 221 mg/ml) were prepared in 500 mM MES buffer and pre-incubated in a water-bath at 30 °C. Each suspension was treated with 40 mM glucose and further incubated at 30 °C. The individual fermentations were stopped at desired intervals by adding 0.2 volume 30 % perchloric acid and immediately freezing in liquid nitrogen [82]. Cell suspensions were then frozen and thawed three times, following which they were centrifuged in an Eppendorf 5804R centrifuge for 20 min at 5000 rpm (4500×g) and 0 °C. The supernatant was retained and was neutralized by adding 2 M potassium carbonate. Samples were then centrifuged again to remove salt and the supernatant retained. Equal volume supernatant from each tube was freeze-dried overnight. The freeze-dried samples were resuspended in 15 %  $\text{D}_2\text{O}$ , 1 mM TEP (internal standard [83]) and 30 mM sodium-EDTA (pH 8.2). EDTA improves stability of adenine nucleotides in cell extracts.



### 5.3.2 In vitro phosphate-metabolite measurements

The resuspended extracts were analysed overnight at 161.9 MHz on a 400 MHz Varian spectrometer. Each sample was run for 19300 scans per data-point, with the following parameters: pulse width = 3.1  $\mu$ s, relaxation delay = 1 s, acquisition time = 1.6 s, spectral width from -60 to 60 ppm. Each data-point is a cumulative representation of all the scans taken over a  $\pm$  14 hour-period.

### 5.3.3 ATP/ADP ratios from NMR data

The phosphate peaks, as identified by means of the standards (Figures 2.4-2.6), were integrated using the 1D graphic interface program MestreNova 6.2.0 software's manual integration tool [81]. This integration of peaks, representing intensity of signal for each type of phosphate nucleus, can be used to calculate concentrations by comparing peak area to that of the internal standard, triethyl phosphate (TEP) [83]. The ratio between the average intensities of the ATP peaks and the ADP peaks (ATP/ADP) was calculated as a representation of the energy state of the cells. Peak intensities were again calibrated for relaxation times, as described in Chapter 2.

## 5.4. Supply-demand analysis

The natural logarithms of the glucose and lactate fluxes (as determined by NMR spectroscopy upon titration with sodium acetate) were plotted as a function the natural logarithm of the ATP/ADP. The gradient of the resulting curve represents the elasticity of the supply pathway (glucose and lactate flux) to changes in ATP/ADP. Elasticity coefficients were calculated as follows:

$$\epsilon_{\text{ATP/ADP}}^{J_{\text{glc}}} = \delta \ln J_{\text{glc}} / \delta \ln (\text{ATP/ADP}) \quad [\text{Eq. 33}]$$

$$\epsilon_{\text{ATP/ADP}}^{J_{\text{lac}}} = \delta \ln J_{\text{lac}} / \delta \ln (\text{ATP/ADP}) \quad [\text{Eq. 34}]$$

## REFERENCES

1. Beukes, E., Bester, B. H. & Mostert, J. F. (2001) The microbiology of South African traditional fermented milks. *International Journal of Food Microbiology*, 63: 189-197.
2. Soomro, A. H., Masud, T. & Anwaar, K. (2002) Role of lactic acid bacteria (LAB) in food preservation and human health – a review. *Pakistan Journal of Nutrition*, 1 (1): 20-24.
3. Savadogo, O. C. S. P. O. A. B. N. & Traore, A. (2004) Microorganisms Involved in Fulani Traditional Fermented Milk in Burkina Faso. *Pakistan Journal of Nutrition*, 3 (2): 134-139.
4. Ward, A. (1898) The Persistence of Bacteria in the Milk Ducts of the Cow's Udder. *Transactions of the American Microscopical Society*, 20: 57-68.
5. Donkor, E.S., Aning, K.G. & Quaye, J. (2007) Bacterial contaminations of informally marketed raw milk in Ghana. *Ghana Medical Journal*, 41 (2): 58-61.
6. Ekici, K., Bozkurt, H. & Isleyici, O. (2004) Isolation of Some Pathogens from Raw Milk of Different Milch Animals. *Pakistan Journal of Nutrition*, 3 (3): 161-162.
7. Gaya, P., Medina, M., Bautista, L. & Nunez, M. (1988) Influence of lactic starter inoculation, curd heating and ripening temperature on *Staphylococcus aureus* behaviour in Manchego cheese. *International Journal of Food Microbiology*, 6: 249-257.
8. <http://www.dairyscience.info/bacteriophage-control.html?start=5>
9. Stackebrandt, E. & Teuber, M. (1988) Molecular taxonomy and phylogenetic position of lactic acid bacteria. *Biochimie*, 70 (3): 317-324.
10. Koebmann, B. J., Andersen, H. W., Solem, C. & Jensen, P. R. (2002) Experimental determination of control of glycolysis in *Lactococcus lactis*. *Antonie van Leeuwenhoek*, 82: 237-248.
11. Salama, M. S., Musafija-Jeknic, T., Sandine, W. E. & Giovannoni, S. J. (1995) An ecological study of lactic acid bacteria: isolation of new strains of *Lactococcus* including *Lactococcus lactis* subspecies *cremoris*. *Journal Dairy Science*, 78: 1004-1017.

12. Voit, E. O., Almeida, J., Marino, S., Lall, R., Goel, G., Neves, A. R. & Santos, H. (2006) Regulation of glycolysis in *Lactococcus lactis*: an unfinished systems biological case study. *IEE Proceedings - Systems Biology*, 153 (4): 286-298.
13. Rallu, F., Gruss, A., Ehrlich, D. & Maguin, E. (2000) Acid- and multistress-resistant mutants of *Lactococcus lactis*: identification of intracellular stress signals. *Molecular Microbiology*, 35 (3): 517-528.
14. Schleifer, K. H., Kraus, J., Dvorak, C., Kilper-Baelz, R., Collins, M. D. & Fischer, W. (1985) Transfer of *Streptococcus lactis* and related streptococci to the genus *Lactococcus* gen. nov. *Systematic and Applied Microbiology*, 6 (2): 183-195.
15. Wegmann, U., O'Connell-Motherway, M., Zomer, A., Buist, G. Shearman, C., Canchaya, C., Ventura, M., Goesmann, V., Gasson, M. J., Kuipers, O. P., van Sinderen, D. & Kok, J. (2007) Complete genome sequence of the prototype lactic acid bacterium *Lactococcus lactis* ssp. *cremoris* MG1363. *Journal of Bacteriology*, 189 (8): 3256-3270.
16. Kim, W. S., Ren, J. & Dunn, N. W. (2001) Assessment of the tolerance of *Lactococcus lactis* cells at elevated temperatures. *Biotechnology Letters*, 23: 1141-1145.
17. Bergère, J.-L., Hermier, J. & Lacourt, A. (1968) La production massive de cellules de streptocoques lactiques.II. -Croissance de "*Streptococcus lactis*" dans un milieu a pH constant. *Lait*, 48 (471-472): 13-30.
18. Bibal, B., Goma, G., Vayssier, Y. & Pareilleux, A (1988) Influence of pH, lactose and lactic acid on the growth of *Streptococcus cremoris*: a kinetic study. *Applied Microbiology and Biotechnology*, 28 (4-5): 340-344.
19. Harvey, R. J. (1965) Damage to *Streptococcus lactis* resulting from growth at low pH. *Journal of Bacteriology*, 90: 1330.
20. Even, S., Lindley, N. D. & Cocaign-Bousquet, M. (2003) Transcriptional, translational and metabolic regulation of glycolysis in *Lactococcus lactis* subsp. *cremoris* MG1363 grown in continuous acidic cultures. *Microbiology*, 149: 1935-1944.

21. Cocaign-Bousquet, M., Even, S.; Lindley, N. D. & Loubiere, P. (2002) Anaerobic sugar catabolism in *Lactococcus lactis*: genetic regulation and enzyme control over pathway flux. *Applied Microbiology and Biotechnology*, 60: 24-32.
22. Hoefnagel, M. H. N., van der Burgt, A., Martens, D. E., Hugenholtz, J. & Snoep, J. L. (2002) Time-dependent responses of glycolytic intermediates in a detailed glycolytic model of *Lactococcus lactis* during glucose run-out experiments. *Molecular Biology Reports*, 29: 157-161.
23. Neijssel, O. M., Snoep, J. L. & de Mattos, M. J. T. (1997) Regulation of energy source metabolism in streptococci. *Journal of Applied Microbiology Symposium Supplement*, 83: 12S-19S.
24. Garrigues, C., Loubiere, P., Lindley, N. D. & Cocaign-Bousquet, M. (1997) Control of the shift from homolactic acid to mixed-acid fermentation in *Lactococcus lactis*: Predominant role of the NADH/NAD<sup>+</sup> ratio. *Journal of Bacteriology*, 179 (17): 5282-5287.
25. Thomas, T. D., Ellwood, D. C. & Longyear, V. M. C. (1979) Change from homo- to heterolactic fermentation by *Streptococcus lactis* resulting from glucose limitation in anaerobic chemostat cultures. *Journal of Bacteriology*, 138: 109-117.
26. Thomas, T. D., Turner, K. W. & Crow, V. L. (1980) Galactose fermentation by *Streptococcus lactis* and *Streptococcus cremoris*: Pathways, Products and Regulation. *Journal of Bacteriology*, 144 (2): 672-682.
27. Starrenberg, M. J. C. & Hugenholtz, J. (1991) Citrate fermentation by *Lactococcus* and *Leuconostoc* spp. *Applied and Environmental Microbiology*, 55: 3535-3540.
28. Solem, C., Koebmann, B., Yang, F. & Jensen, P. R. (2007) The las enzymes control pyruvate metabolism in *Lactococcus lactis* growth on maltose. *Journal of Bacteriology*, 189 (18): 6727-6730.
29. Sjoberg, A. & Hahn-Hagerdal, B. (1989) B-3-Glucose-1-Phosphate, a possible mediator for polysaccharide formation in maltose-assimilating *Lactococcus lactis*. *Applied and Environmental Microbiology*, 55 (6): 1549-1554.
30. Hoefnagel, M. Starrenberg, M., Martens, D., Hugenholtz, J., Kleerebezem, M., Swam, I. V., Bongers, R., Westerhoff, H. & Snoep, J. (2002) Metabolic engineering of lactic acid bacteria, the combined approach: kinetic modelling, metabolic control

- analysis and experimental analysis. *Microbiology*, 148: 1003-1013. Available online: <http://jjj.biochem.sun.ac.za/webMathematica/Examples/run.jsp?modelName=hoefnagel1>
31. <http://jjj.biochem.sun.ac.za/webMathematica/Examples/run.jsp?modelName=hoefnagel2>
  32. Mendes, P. (1997) Biochemistry by numbers: simulation of biochemical pathways with Gepasi 3. *Trends in Biochemical Science*, 22: 361-363.
  33. Hucka, M., Finney, A., Bornstein, B. J., Keating, S. M., Shapiro, B. E., Matthews, J., Kovitz, B. L., Schilstra, M. J., Funahashi, A., Doyle J. C. & Kitano, H. (2004) Evolving a lingua franca and associated software infrastructure for computational systems biology: the Systems Biology Markup Language (SBML) project. *Systematic Biology*, 1 (1): 41-53.
  34. Hucka, M., Finney, A., Sauro, H. M., Bolouri, H., Doyle, J. C., Kitano, H., and the rest of the SBML Forum: Arkin, A. P., Bornstein, B. J., Bray, D., Cornish-Bowden, A., Cuellar, A. A., Dronov, S., Gilles, E. D., Ginkel, M., Gor, V., Goryanin, I. I., Hedley, W. J., Hodgman, T. C., Hofmeyr, J.-H., Hunter, P. J., Juty, N. S., Kasberger, J. L., Kremling, A., Kummer, U., Le Novère, N., Loew, L. M., Lucio, D., Mendes, P., Minch, E., Mjolsness, E. D., Nakayama, Y., Nelson, M. R., Nielsen, P. F., Sakurada, T., Schaff, J. C., Shapiro, B. E., Shimizu, T. S., Spence, H. D., Stelling, J., Takahashi, K., Tomita, M., Wagner, J. & Wang, J. (2003) The systems biology markup language (SBML): a medium for representation and exchange of biochemical network models. *Bioinformatics*, 19 (4): 524-531.
  35. Kacser, H. & Burns, J. A. (1973) The control of flux. *Symposium for the Society of Experimental Biology*, 27, 65-104.
  36. Kacser, H. & Burns, J. A. (1979) Molecular democracy: who shares the controls? *Biochemical Society Transactions*, 7, 1149-1160.
  37. Fell, D. A. (1992) Metabolic control analysis: a survey of its theoretical and experimental development. *Biochemical Journal*, 286: 313-330.
  38. Heinrich, R. & Rapoport, T. A. (1974) A linear steady state treatment of enzymatic chains. *European Journal of Biochemistry*, 42, 89-95, 97-105.

39. Kahn, D. & Westerhoff, H. V. (1991) Control theory of regulatory cascades. *Journal of Theoretical Biology*, 153 (2): 255-285.
40. Hofmeyr, J. S. & Cornish-Bowden, A. (2000) Regulating the cellular economy of supply and demand. *FEBS Letters*, 476: 47-51.
41. Kroukamp, O., Hofmeyr, J. S., Rohwer, J. M. & Snoep, J. L. (2002) Experimental supply-demand analysis of anaerobic yeast energy metabolism. *Molecular Biology Reports*, 29 (1-2): 203-209.
42. Koebmann, B., Solem, C., Pedersen, M., Nilsson, D. & Jensen, P. (2002) Expression of genes encoding F<sub>1</sub>-ATPase results in uncoupling of glycolysis from biomass production in *Lactococcus lactis*. *Applied and Environmental Microbiology*, 68(9): 4274-4282.
43. Poolman, B., Bosman, B., Kiers, J. & Konings, W. N. (1987) Control of glycolysis by glyceraldehyde-3-phosphate dehydrogenase in *Streptococcus cremoris* and *Streptococcus lactis*. *Journal of Bacteriology*, 169 (12): 5887-5890.
44. Even, S., Garrigues, C. Loubiere, P. Lindley, N. D. & Cocaign-Bousquet, M. (1999) Pyruvate metabolism in *Lactococcus lactis* is dependent upon glyceraldehyde-3-phosphate dehydrogenase activity. *Metabolic Engineering*, 1 (3): 198-205.
45. Andersen, H. W., Solem, C., Hammer, K. & Jensen, P. R. (2001) Lactate dehydrogenase has no control on lactate production but has a strong negative control on formate production in *Lactococcus lactis*. *European Journal of Biochemistry*, 268: 6379-6389.
46. Wolin, M. J. (1964) Fructose-1,6-disphosphate requirement of streptococcal lactic dehydrogenases. *Science*, 146 (3545): 775-777.
47. Andersen, H. W., Solem, C., Hammer, K. & Jensen, P. R. (2001) Twofold reduction of phosphofructokinase activity in *Lactococcus lactis* results in strong decreases in growth rate and glycolytic flux. *Journal of Bacteriology*, 183 (11): 3458-3467.
48. Collins, L. B. & Thomas, T. D. (1974) Pyruvate kinase of *Streptococcus lactis*. *Journal of Bacteriology*, 120 (1): 52-58.
49. Ramos, A., Neves, A. R., Ventura, R., Maycock, C., Lopez, P. & Santos, H. (2004) Effect of pyruvate kinase overproduction on glucose metabolism of *Lactococcus lactis*. *Microbiology*, 150: 1103-1111.

50. Yamada, T. & Carlsson, J. (1975) Regulation of lactate dehydrogenase and change of fermentation products in streptococci. *Journal of Bacteriology*, 124 (1): 55-61.
51. Kobayashi, H. (1985) A proton-translocating ATPase regulates pH of the bacterial cytoplasm. *Journal of Biological Chemistry*, 260 (1): 72-76.
52. Futai, M. & Kanazawa, H. (1983) Structure and function of proton-translocating adenosine triphosphatase (F<sub>0</sub>F<sub>1</sub>): biochemical and molecular biological approaches. *Microbiological Reviews*, 47 (3): 285-312.
53. Koebmann, B. J., Nilsson, D., Kuipers, C. P. & Jensen, P. R. (2000) The Membrane-Bound H<sup>+</sup>-ATPase Complex Is Essential for Growth of *Lactococcus lactis*. *Journal of Bacteriology*, 182 (17): 4738-4743.
54. Kobayashi, H., Suzuki, T. & Unemoto, T. (1986) Streptococcal cytoplasmic pH is regulated by changes in amount and activity of a proton-translocating ATPase. *Journal of Biological Chemistry*, 261 (2): 627-630.
55. Koebmann, B. J., Westerhoff, H. V., Snoep, J. L., Nilsson, D. & Jensen, P. R. (2002) The glycolytic flux in *Escherichia coli* is controlled by the demand for ATP. *Journal of Bacteriology*, 184 (14): 3909-3916.
56. Cock, L. S. & de Stouvenel, A. R. (2006) Lactic acid production by a strain of *Lactococcus lactis* ssp *lactis* isolated from sugar cane plants. *Electronic Journal of Biotechnology*, 9 (1): 40-45.
57. Emsley, J. W. & Feeney, J. (1995) Milestones in the first fifty years of NMR. *Progress in Nuclear Magnetic Spectroscopy*, 28: 1-9.
58. Akitt, J. & Mann, B. (2000) NMR and Chemistry: an introduction to modern spectroscopy. Taylor & Francis Group, *Chapman & Hall*.
59. Roberts, J. (2000) ABCs of FT-NMR. *University Science Books*.
60. Gadian, D. G. (2002) NMR and its application to living systems. *Oxford University Press*.
61. Barbotin, J-N. and Porta, J-C. (2000) NMR in Microbiology: theory and application., *Horizon Scientific Press, Wymondham, UK*.
62. Cohen, J. S., Jaroszewski, J. W., Ruiz-Cabello, O. K. J. & Collier, S. W. (1995) A history of biological applications of NMR spectroscopy. *Progress in Nuclear Magnetic Spectroscopy*, 28: 53-85.

63. Neves, A. R., Ramos, A., Nunes, M. C., Kleerebezem, M., Hugenholtz, J., de Vos, W. M., Almeida, J. & Santos, H. (1999) *In vivo* nuclear magnetic resonance studies of glycolytic kinetics in *Lactococcus lactis*. *Biotechnology and Bioengineering*, 64 (2): 200-212.
64. Evans, J. N. (1995) *Biomolecular NMR Spectroscopy*. Oxford University Press.
65. Le Bourgeois, P., Lautier, M., van der Berghe, L. Gasson, M. and Ritzenhaler, P. (1995) Physical and genetic map of the *Lactococcus lactis* ssp *cremoris* MG1363 chromosome: comparison with that of *Lactococcus lactis* ssp *cremoris* IL1403 reveals a large genome inversion. *Journal of Bacteriology*, 177 (10), 2840-2850.
66. Smith, G. M., Byung, W. K., Franke, A. A., Roberts, J. D. (1985) <sup>13</sup>C NMR Studies of Butyric Fermentation in *Clostridium kluyveri*. *Journal of Biological Chemistry*, 260 (25), 13509-13512.
67. Elango, G., Guhanathan, S. and Venkataraman, T. (2010) 2,3-butanediol based liquid crystalline random copolyester, synthesis and characterisation. *International Journal of Physical Sciences*, 5 (13): 2104-2117.
68. Mercade, M., Lindley, N. D. and Loubiere, P. (2000) Metabolism of *Lactococcus lactis* subsp. *cremoris* MG 1363 in acid stress conditions. *International Journal of Food Microbiology*, 55: 161-165.
69. Even, S., Lindley, N. D., Loubiere, P. and Cocaign-Bousquet, M. (2002) Dynamic response of catabolic pathways to auto-acidification in *Lactococcus lactis*: transcript profiling and stability in relation to metabolic and energetic constraints. *Molecular Microbiology*, 45 (4): 1143-1152.
70. Kacser, H. and Burns, J. A. (1995) The control of flux: 21 years on. *Biochemical Society Transactions*, 23, 341-366.
71. Smith, J.A. (2010) Experimental supply demand analysis of yeast fermentation free energy metabolism: an *in vivo* and *in situ* investigation. Thesis submitted to the University of Stellenbosch for the degree Masters of Science.
72. Du Preez, F. B., Conradie, R., Penkler, G. R., Holm, K., van Dooren, F. L. J. & Snoep, J. L. (2008) A comparative analysis of kinetic models of erythrocyte glycolysis. *Journal Theoretical Biology*, 252: 488-496.



73. Koebmann, B. J., Nilsson, D., Kuipers, O. P. and Jensen, P. R. (2000) The Membrane-bound H<sup>+</sup>-ATPase complex is essential for growth of *Lactococcus lactis*. *Journal of Bacteriology*, 182(7): 4738-4743.
74. Kushkel, E. R. (1987) Bioenergetics of lactic acid bacteria: cytoplasmic pH and osmotolerance. *FEMS Microbiology Letters*, 43 (3), 233-244.
75. Even, S., Lindley, N. D., Loubierre, P. & Cocaïgn-Bousquet, M. (2002) Dynamic response of catabolic pathways to auto-acidification in *Lactococcus lactis*: transcript profiling and stability in relation to metabolic and energy constraints, *Molecular Microbiology*, 45 (4), 1143-1152.
76. Andersen, A. Z., Carvalho, A. L., Neves, A. R., Santos, H., Kummer, U. & Olsen, L. F. (2009) A metabolic pH response in *Lactococcus lactis*: an integrative experimental and modelling approach. *Computational Biology & Chemistry*, 33, 71-83.
77. Llanos, R. M., Harris, C. J., Hillier, A. J. and Davidson, B. E. (1993) Identification of a novel operon in *Lactococcus lactis* encoding three enzymes for lactic acid synthesis: phosphofructokinase, pyruvate kinase, and lactate dehydrogenase. *Journal of Bacteriology*, 175, 2541-2551.
78. Solem, C. and Jensen, P. R. (2002) Gene modulation made easy. *Applied and Environmental Microbiology*, 68 (5): 2397-2403.
79. Solem, C., Koebmann, B., Fang, Y. and Jensen, P. R. (2007) The *las* enzymes control pyruvate metabolism in *Lactococcus lactis* during growth on maltose. *Journal of Bacteriology*, 189 (18): 6727-6723.
80. de Man, J.D., Rogosa, M. & Sharpe, M.E. (1960) A medium for the cultivation of "*Lactobacilli*". *Journal of Applied Bacteriology*, 23: 130-135.
81. [www.mestrelab.com](http://www.mestrelab.com)
82. Barrow, K. D., Collins, J. G., Norton, R. S., Rogers, P. L. & Smith, G. M. (1984) <sup>31</sup>P nuclear magnetic resonance studies of the fermentation of glucose to ethanol by *Zymomonas mobilis*. *Journal of Biological Chemistry*, 259 (9): 5711-5716.
83. Kirk, K. & Kuchel, P. (1988) Characterization of transmembrane chemical shift differences in the <sup>31</sup>P NMR spectra of various phosphoryl compounds added to erythrocyte suspensions. *Biochemistry*, 27 (24): 8795-8802.